Dynamic Studies of Excited-State Proton Transfer to Solvent from Phenol and Its Derivatives in Water

Shigeo KANEKO

Contents

Chapter I

Introduction

I-1   *Excited-state proton transfer reactions in biological systems*

Proton transfer is one of the most fundamental processes in chemistry and biochemistry [1-5]. Until recently, much attention has been paid to photo-induced proton transfer reactions because of its importance in fundamental aspects of reaction dynamics [2] and also of various possibilities for applications [3,6,7]. Proton transfer reactions in the excited state of aromatic compounds have been found in some biological systems such as anthocyanins [8], green fluorescent protein (GFP) [9-12], and so on [13,14]. GFP is well known as a powerful tool that has recently enabled to study dynamic molecular events within living cells [15,16]. The intrinsic fluorescence from protein upon ultra-violet (UV) excitation is an important probe for studying their dynamic properties and interactions with other biomolecules.

3-Hydroxyflavone shown in Figure I-1 is known as a biological photoacid that undergoes intramolecular proton transfer in the excited state [17]. Flavonoids are a group of polyphenolics, which are present in virtually all land-based plants. They display strong absorption in the UV spectral region and the flavonols, that is, 3-hydroxyflavones, exhibit fluorescence with absorption maxima at about 350-370 nm. It has been suggested that protection against UVB-induced damage may be an important function of flavonols in plants [18]. There have been some industrial applications as efficient UV absorber using the intramolecular proton transfer [19]. In case of 7-hydroxyquinoline, intramolecular water-assisted proton transfer is observed in the excited state [20] (see Figure I-1). Proton relay transfer may serve as experimental model for proton relays and proton pumps for transport of protons across membranes in biological systems [20].

Anthocyanins and 10-hydroxycamptothecin shown in Figure I-2 are biological

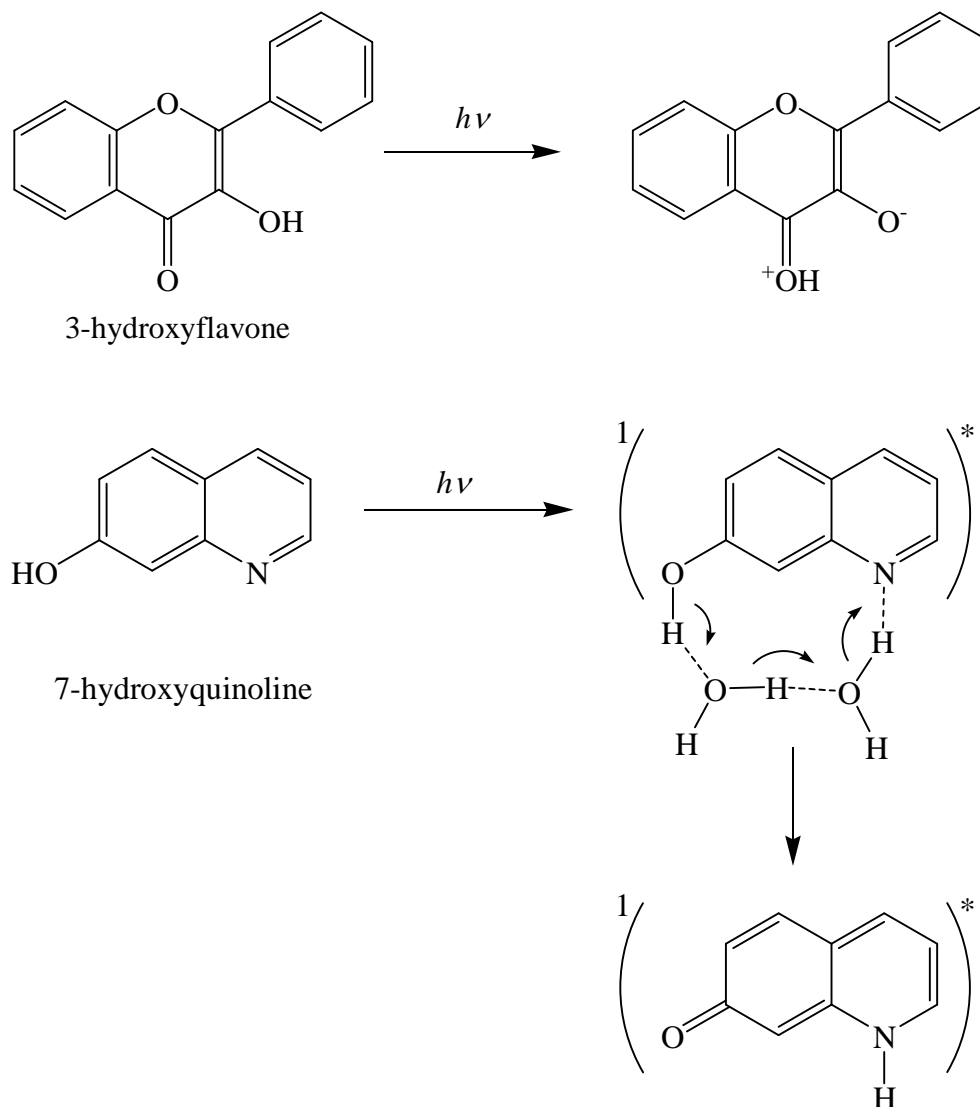**Figure I-1.** Biological compounds showing excited-state intramolecular proton transfer

cyanin

malvin

pelargonin

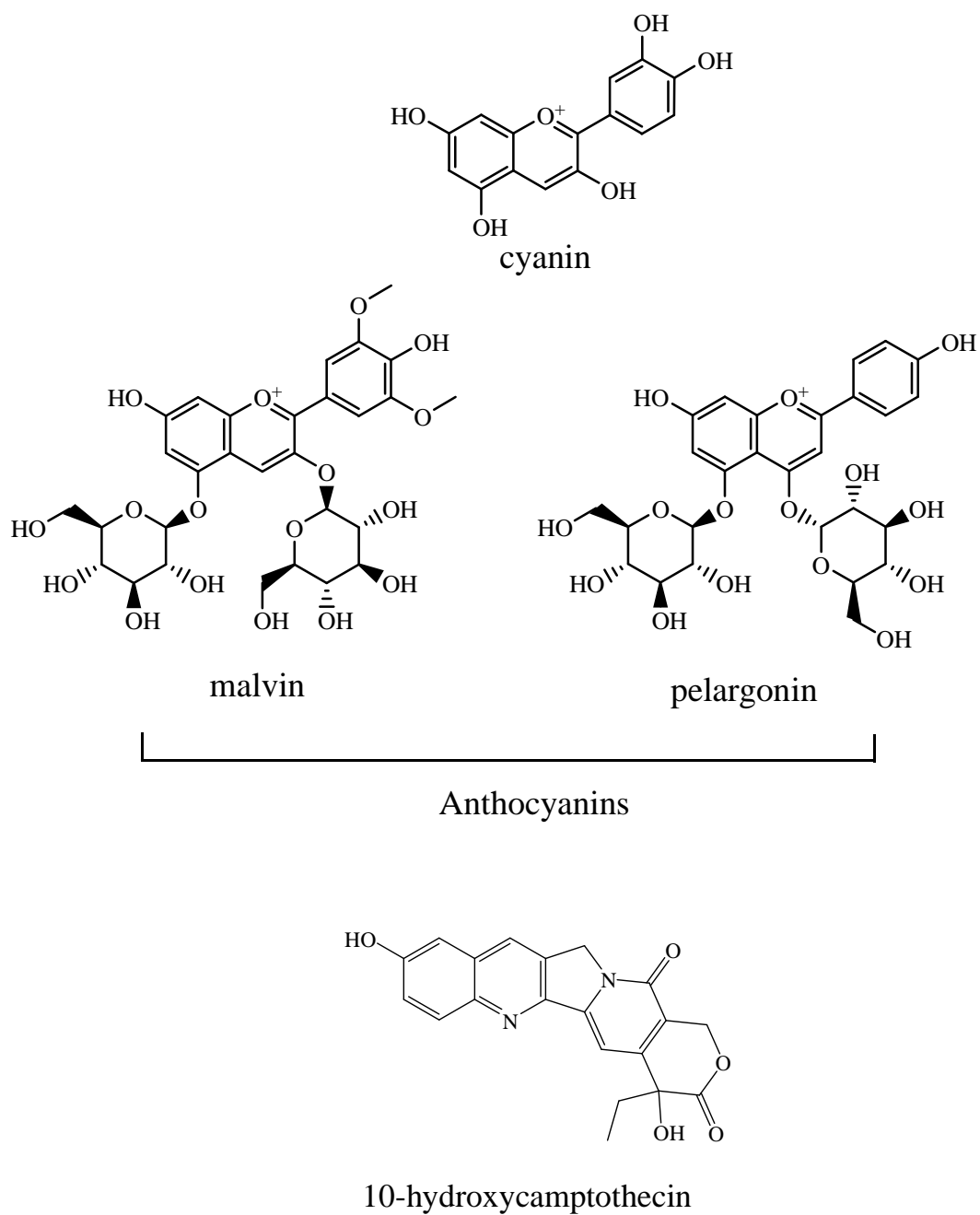Anthocyanins

10-hydroxycamptothecin

Figure I-2. Biological compounds showing excited-state intermolecular proton transfer

4

photoacid derivatives which exhibit intermolecular proton transfer reactions in the excited state. Malvin, cyanin, and pelargonin are among the most representative anthocyanins because of their abundance in the most common red flowers and fruits [8]. It is known that natural anthocyanins such as Figure I-2 undergo ultrafast intermolecular proton transfer to water in the excited state [8]. This excited-state proton transfer (ESPT) process is highly efficient as an energy-wasting mechanism, as would be required by an in vivo role such as protection of plant tissues from potentially deleterious excess radiant energy.

The ESPT reactions are also reported for phenol derivatives such as *trans-o*-hydroxycinnamic acid and *p*-hydroxybenzylidene-dimethylimidazolidone (see Figure I-3). These compounds show green fluorescence resulting from ESPT reactions, although the quantum yield of the green fluorescence is significantly small in solution. Cinnamic acids are well known to widespread in nature. A derivative of the cinnamic acids, *trans-o*-hydroxycinnamic acid, has also been reported to show excited-state intermolecular proton transfer [21]. As shown in Figure I-4, *p*-hydroxybenzylidene-dimethylimidazolidone plays an important role as fluorophore of green fluorescent protein (GFP) which is now widely used as noninvasive, genetically encoded reporters in biochemistry and cell biology [15,16]. It has been suggested that, in wild-type GFP (wtGFP), not only the deprotonated form of the chromophore but also the protonated form, which exhibits an absorption peak at 398 nm, gives the characteristic green emission resulting from the ESPT reaction to water molecules in the vicinity of the chromophore in GFP [9-12].
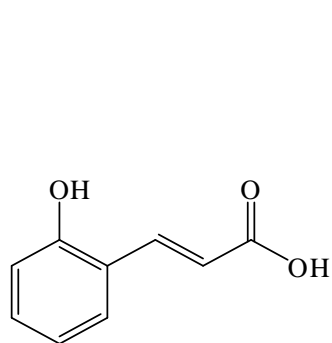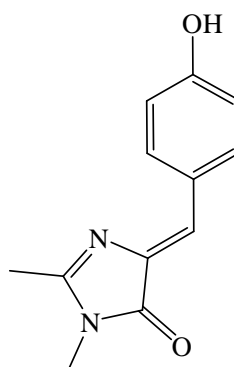
trans-*o*-hydroxycinnamic acid   *p*-hydroxybenzylidene-dimethylimidazolinone

Figure I-3.   Molecular structures of *trans-o*-hydroxycinnamic acid and *p*-hydroxybenzylidene-dimethylimidazolinone
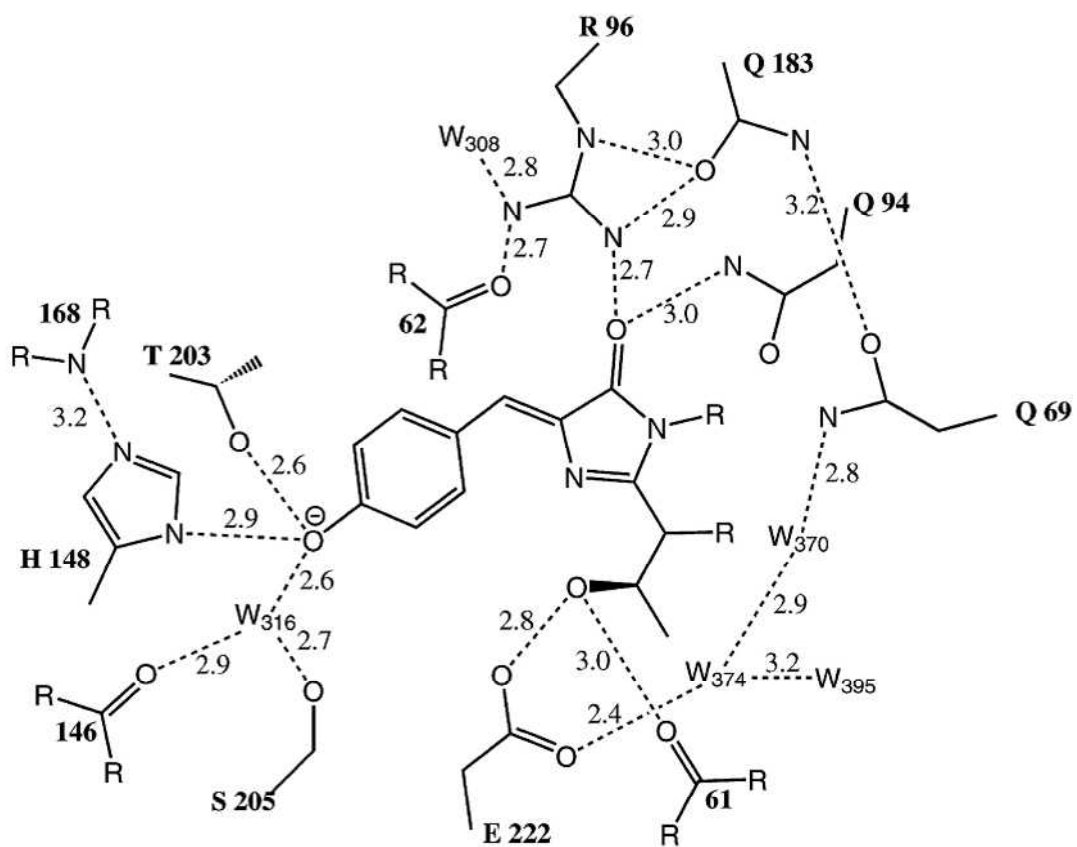
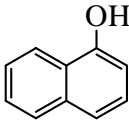**Figure I-4.** Structure of the emitting site in wild-type GFP
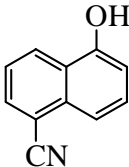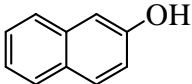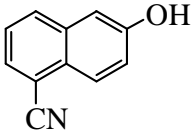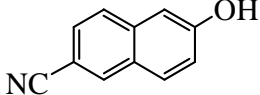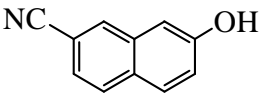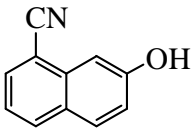
I-2   *ESPT reactions of hydroxyarenes*

As exemplified in the previous section, in biological systems, ESPT reaction is usually observed in hydroxyarenes (ROH) which consist of hydroxyl group(s) and aromatic chromophore (R). The ESPT reactions of hydroxyarenes are, therefore, of great importance not only from fundamental aspects of reaction dynamics but also in biological studies. Among hydroxyarenes, ESPT reactions have been studied for 1- and 2-naphthol and their derivatives for more than half a century [27-33].

Naphthols undergo extensive charge redistribution in the excited singlet state both prior and after the proton transfer reaction. The aromatic residue may be viewed as becoming more electronegative in the excited state, shifting some electron density away from the O atom. Such intramolecular charge redistribution processes are usually assumed to be stabilized by polar solvents. The increased acidity of the OH hydrogen atom of naphthols may eventually result in a full charge separation (proton-transfer reaction). For such a reaction to proceed with a detectable speed it must be carried out in a polar solvent that can stabilize both the proton and the aromatic anion. In dilute solutions, the dissociation of neutral photoacids such as naphthols generates isolated ion pairs for time durations, which are longer than the excited-state lifetime of the photoacid.

In Table I-1, the reported values for the acidity constant of naphthols in both ground state (pK_a) and the lowest excited singlet (S_1) state (pK_a*) are listed together with the proton-dissociation rate constant (k_{dis}) in the S_1 state. It is noted from Table I-1 that the acidity of these compounds increases dramatically upon electronic excitation, and the proton dissociation rate in the S_1 state are significantly affected by the introduction of strongly electron-withdrawing cyano group.

Table -1 pK_a, pK_a^* and k_{dis} values of aromatic hydroxy compounds.

Compound	pK_a	pK_a^*	k_{dis} $(10^{10}\,s^{-1})$
(1-naphthol, OH)	9.23^c	2.0^c	2.5^a
(OH / CN naphthalene)	-	-2.8^f	13^f
(2-naphthol, OH)	9.5^b	2.8^c	$1.0\times10^{-2\,e}$
(OH / CN naphthalene)	8.75^b	-1.2^b	7^d
(NC / OH naphthalene)	8.4^b	0.2^b	1.1^d
(NC / OH naphthalene)	8.75^b	-1.3^b	$5.5\times10^{-1\,d}$
(CN / OH naphthalene)	8.35^b	-0.4^b	$2.7\times10^{-1\,d}$

[a] Ref. 34
[b] Ref. 35
[c] Ref. 36
[d] Ref. 37
[e] Ref. 38
[f] Ref. 39

I-3 *Geminate recombination reaction in ion-pair produced by ESPT reactions*

To fully understand the dynamics of ESPT reactions, it is required to clarify the geminate recombination of the ion-pair (RO$^{-*}\cdots$H$^+$) following proton dissociation in the excited state. In the case of hydroxyarenes which undergo ESPT reactions, a long-time tail can be detected in the fluorescence decay profile. As a typical example, the logarithmic fluorescence decay profiles of 1-naphthol (NpOH) and 1-naphtholate anion (NpO$^-$) produced by ESPT reaction in H$_2$O are presented in Figure I -5. The fluorescence decay profile of NpOH exhibits a long-time tail following tens of picosecond decay due to proton dissociation in the S$_1$ state.

The kinetics of the geminate recombination can be represented by the following reaction scheme:

$$\text{ROH}^* \; \underset{k_r(t)}{\overset{k_d}{\rightleftharpoons}} \; [\text{RO}^{*-}...\text{H}^+]_{(r=a)} \overset{\text{DSE}}{\Longrightarrow} [\text{RO}^{*-}+\text{H}^+]_{(r\quad)} \tag{I-1}$$
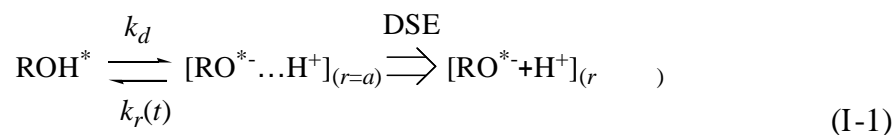
The ions recombine before their mutal distancec become greater than the radius of the Coulomb cage. The rate constant for geminate recombination $k_r(t)$ is time-dependent and can be approximated to follow $t^{-3/2}$ at long times [22-26]. In restricted media, the long-time tail is even longer because of the higher probability of recapturing a photoejected proton by geminate recombination.
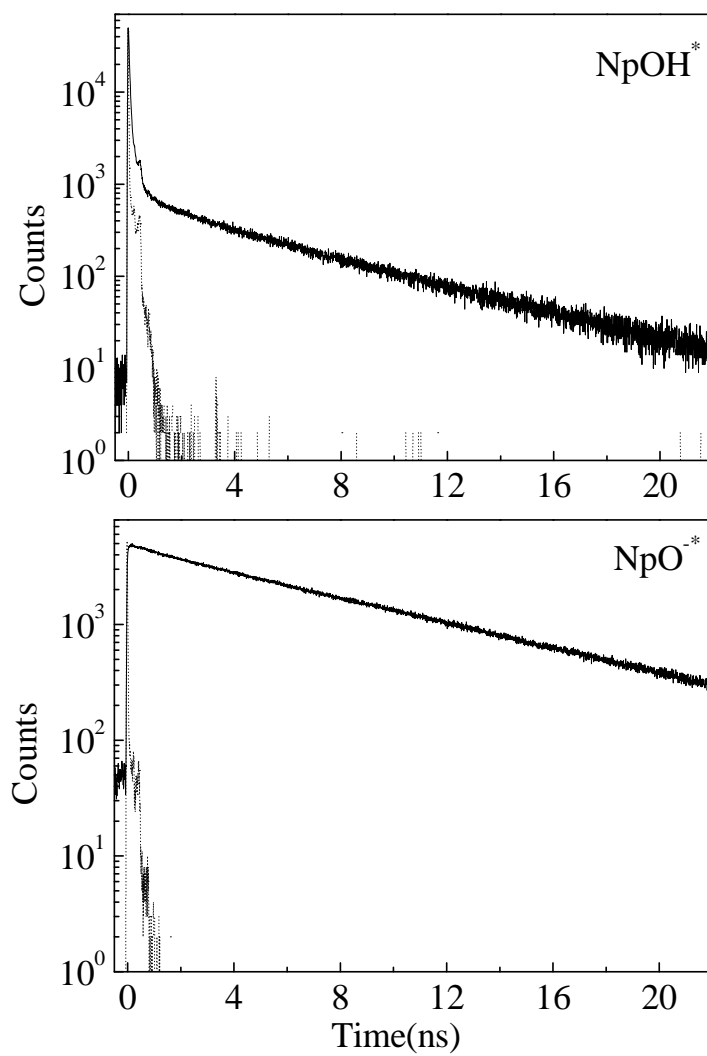
Figure I-5. Fluorescence time profiles of NpOH* and NpO⁻* in H₂O at 293 K.

I-4 *Purpose of this study*

During past several decades, studies on excited-state intermolecular proton transfer reactions of hydroxyarenes have been carried out mainly on 1- and 2-naphthols, because in these molecules, both neutral (ROH) and deprotonated anion (RO⁻) give relatively strong fluorescence. As a result, 1- and 2-naphthols in water show dual fluorescence, shorter- and longer wavelength fluorescence bands, originating from excited states of protonated and deprotonated species, respectively. The appearance of such dual fluorescence is generally used as indication of occurrence of ESPT reactions.

As described in section I-1, phenol and its derivatives are also very important proton-transfer systems, especially in biological studies. In spite of the fundamental nature and importance in biology, there have been few studies on the dynamics of ESPT reactions of phenols, probably due to the very weak fluorescence both from the parent neutral and the deprotonated anion. Even at the present time, it is not clarified whether phenol in water undergoes proton dissociation in the S_1 state.

In this thesis, excited-state proton transfer reactions of phenol and its derivatives (*o*-, *m*-, and *p*-trifluoromethylphenols and *o*-, *m*-, and *p*-cyanophenols) in water are investigated by means of steady-state and time-resolved fluorescence spectroscopy and time-resolved photoacoustic technique to reveal (1) the occurrence of ESPT reactions in these compounds, (2) substituent effects on the rate of proton transfer from phenols to solvent water, (3) the contribution of geminate recombination reactions in ESPT processes, and (4) the role of solvent in the proton transfer reactions.

References

[1] Shizuka, H. *Acc. Chem. Res.* **1985**, *18*, 141.

[2] Alnaut, L. G.; Formosinho, S. J. *J. Photochem. Photobiol. A: Chem.* **1993**, *75*, 1.

[3] Mishra, A. K. Fluorescence of Excited Singlet State Acids in Certain Organized

 Media: *Applications as Molecular Probes, Eds. V. Ramamurthy and K. S.*

 Schanze, in Understanding and Manipulating Excited State Processes,

 Molecular and Supramolecular Photochemistry Series, Marcel Dekker, Inc.,

 New York, 2001, Vol. 8, Chap. 10.

[4] Tolbert, L. M.; Solntsev, K. M. *Acc. Chem Res.* **2002**, *35*, 19.

[5] Kosower, E. M.; Huppert, D. *Ann. Rev. Phys. Chem.* **1986**, *37*, 127.

[6] Gutman, M.; Nachliel, E. *Annu. Rev. Phys. Che*m., **1997**, *48*, 329.

[7] Moilanen, D. E.; Spray, D. E.; Fayer, M. D. *Langmuir* **2008**, *24*, 3690.

[8] Moreira P. F.; Giestas, L.; Yihwa, C., Vautier-Giongo, C.; Quina, F. H.;

 Maçanita, A. L.; Lima, J. C. *J. Phys. Chem. A* **2003**, *107*, 4203.

[9] Chattoraj, M.; King, B. A.; Bublitz, G. U.; Boxer, S. G. Proc. *Natl. Acad. Sci.*

 U.S.A. **1996**, *93*, 8362.

[10] Stoner-Ma, D.; Jaye, A. A.; Ronayne, K. L.; Nappa, J.; Meech, S. R.; Tonge, P. J.

 J. Am. Chem. Soc. **2008**, *130*, 1227.

[11] Leiderman, P.; Gepshtein, R.; Tsimberov, I.; Huppert, D. *J. Phys. Chem. B* **2008**,

 112, 1232.

[12] Gepshtein, R.; Leiderman, P.; Huppert, D. *J. Phys. Chem. B* **2008**, *112*, 7203.

[13] Genosar, L.; Lasitza, T.; Gepshtein, R.; Leiderman, P.; Koifman, N.; Huppert, D.

 J. Phys. Chem. A **2005**, *109*, 4852.

[14] Solntsev, K. M.; Sullivan, E:; Tolbert, L. M.; Ashkenazi, S.; Leiderman, P.;

Huppert, D. *J. Am. Chem. Soc.*, **2004**, *126*, 12701

[15] Chalfie, M; Kain, S. *Green Fluorescent Protein: Properties, Applications, and Protocols*; Wiley-Liss: New York, 1998.

[16] Tsien, R. Y. *Annu. Rev. Biochem.* **1998**, *67*, 509.

[17] Ameer-Beg, S.; Ormson, S. M.; Brown, R. G.; Matousek, P.; Towrie, M.; Nibbering, E. T. J.; Foggi, P.; Neuwahl, F. V. R. *J. Phys. Chem. A* **2001**, *105*, 3709.

[18] Smith, G. J.; Markham, K. R. *J. Photochem. Photobiol. A* **1998**, *118*, 99.

[19] (a) Lärmer, F.; Elsaesser, T.; Kaiser, W. *Chem. Phys. Lett.* **1988**, *148*, 119. (b) Elsaesser, T.; Lärmer, F.; Frey, W. *Inst. Phys. Conf. Ser.* **1991**, *126*, 543. (c) Wiechmann, M.; Port, H.; Lärmer, F.; Frey, W.; Elsaesser, T. *Chem. Phys. Lett.* **1990**, *165*, 28. (d) Chudoba, C.; Lutgen, S.; Jentzsch, T.; Riedle, E.; Wörner, M.; Elsaesser, T. *Chem. Phys. Lett.* **1995**, *240*, 35.

[20] Kang, W.-K.; Cho, S.-J.; Lee, M.; Kim, D.-H.; Ryoo, R.; Jung, K.-H.; Jang, D.-J. *Bull. Korean Chem. Soc.* **1992**, *13*, 140.

[21] Wolfbeis, O. S.; Begum, M.; Hochmuth, P. *Photochem. Photobiol.* **1986**, *44*, 550.

[22] Pines, E.; Huppert, D. *Chem. Phys. Lett.* **1986**, *126*, 88.

[23] Pines, E.; Huppert, D. *J. Chem. Phys.* **1986**, *84*, 3576.

[24] Agmon, N.; Pines, E.; Huppert, D. *J. Chem. Phys.* **1988**, *88*, 5631.

[25] Pines, E.; Huppert, D.; Agmon, N. *J. Chem. Phys.* **1988**, *88*, 5620.

[26] (a) Agmon, N. *J. Chem. Phys.* **1988**, *89*, 1524. (b) Gopich, I. V.; Solntsev, K. M.; Agmon, N. *J. Chem. Phys.* **1999**, *110*, 2164. (c) Solntsev, K. M.; Huppert, D.; Agmon, N. *Phys. Rev. Lett.* **2001**, *86*, 3427.

[27] Lee, J.; Robinson, G. W.; Webb, S. P.; Philips, L. A.; Clark, J. H. *J. Am. Chem.*

Soc. **1986**, *108*, 6538.

[28] Webb, S. P.; Philips, L. A.; Yeh, S. W.; Tolbert, L. M.; Clark, J. H. *J. Phys. Chem.* **1986**, *90*, 5154.

[29] (a) Robinson, G. W.; Thistlethwaite, P. J.; Lee, J. *J. Phys. Chem.* **1986**, *90*, 4224.

(b) Robinson, G. W. *J. Phys. Chem.* **1991**, *95*, 10386.

[30] Poles, W.; Cohen, B.; Huppert, D.; *Isr. J. Chem.* **1999**, *39*, 347.

[31] Solntsev, K. M.; Huppert, D.; Agmon, N.; Tolbert, L. M. *J. Phys. Chem. A* **2000**, *104*, 4658.

[32] Clower, C.; Solntsev, K. M.; Kowalik, J.; Tolbert, L. M.; Huppert, D. *J. Phys. Chem. A* **2002**, *106*, 3114.

[33] Genosar, L.; Leiderman, P.; Koifman, N.,; Huppert, D. *J. Phys. Chem. A* **2004**, *108*, 1779.

[34] Agmon, N.; Huppert, D.; Masad, A.; Pines, E. *J. Phys. Chem.* **1991**, *95*, 10407.

[35] Tolbert, L. M.; Haubrich, E. *J. Am. Chem. Soc.* **1990**, *112*, 8163.

[36] Ireland, J. F.; Wyatt, P. A. H.; *Adv. Phys. Org. Chem.* **1961**, *1*, 189.

[37] Huppert, D.; Tolbert, L. M.; Linares-Samaniego, S. *J. Phys. Chem. A* **1997**, *101*, 4602.

[38] Alnaut, L. G.; Formosinho, S. J. *J. Photochem. Photobiol. A: Chem.* **1993**, *75*, 21.

[39] Pines, E.; Pines, D., Barak, T.; Magnes, B. Z.; Tolbert, L. M.; Haubrich, J. E. *Ber. Bunsenges. Phys. Chem.* **1998**, *102*, 511.

Chapter II

Experimental

II-1   *Fluorescence quantum yields*

Absorption and fluorescence spectra were recorded on an UV/vis spectrophotometer (Jasco, Ubest-50) and a spectrofluorometer (Hitachi, F-4010), respectively. The fluorescence quantum yield (Φ_f) was determined by comparing the integrated intensities of the fluorescence spectra (*I*), absorbance (*A*) at the excitation wavelength and the refractive index (*n*) of the solvent for sample solutions and those for standard solutions by using the following equation.

$$\Phi_{fX} = \Phi_{fS} \times \frac{I_X A_S n_X^2}{I_S A_X n_S^2} \qquad \text{(II-1)}$$

where X and S stand for sample and standard solutions. The absorbance of sample solution was adjusted to be ~0.1 at excitation wavelength. As the fluorescence standard solutions, phenol in aqueous solution ($\Phi_f = 0.12$) [1] or aniline in cyclohexane ($\Phi_f = 0.17$) [2] was used.

II-2   *Fluorescence lifetimes*

Nanosecond fluorescence lifetimes were measured with a time-correlated single-photon counting fluorimeter (Edinburgh Analytical Instrument, FL-900CDT) which is schematically shown in Figure II-1. A nanosecond pulsed discharge lamp (pulse width: ~1.0 ns; repetition rate: 40 kHz) filled with hydrogen gas was used as the excitation light source. Emission of samples was detected by a photomultiplier tube (PMT; Hamamatsu, R955). The fluorescence time profiles were analyzed by deconvolution with the instrument response function.

Picosecond fluorescence lifetime measurements were made by using a
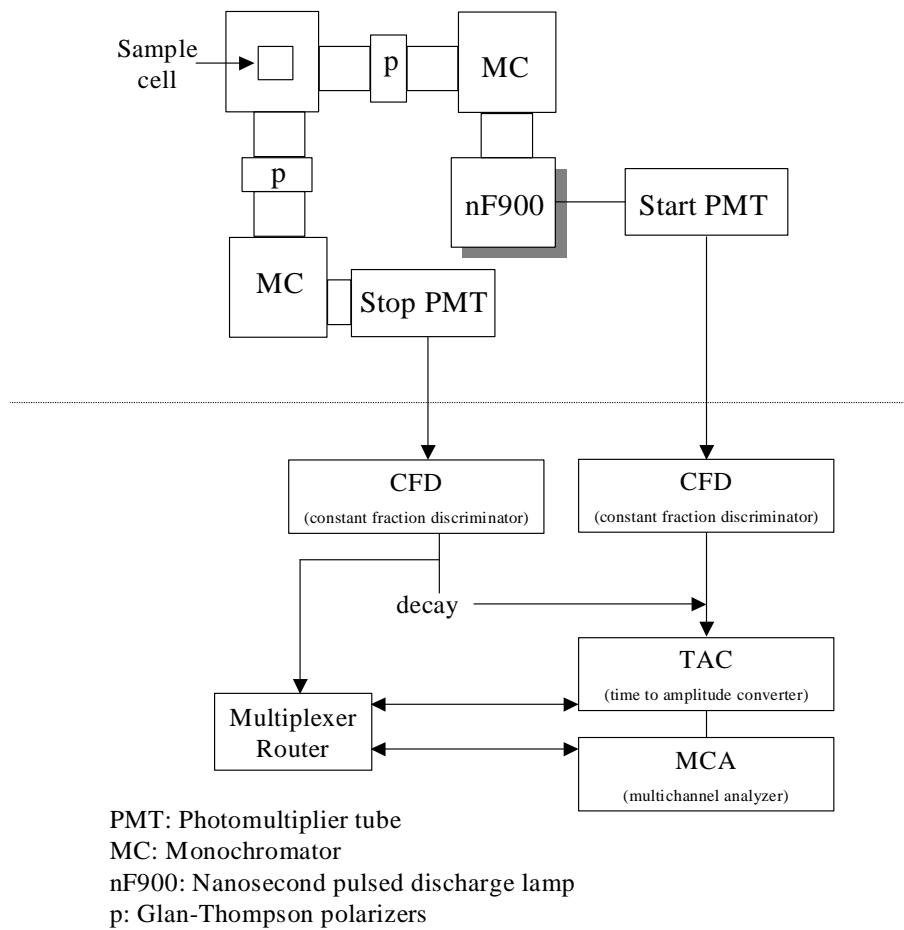
Figure II-1. Schematic diagram of time-correlated single photon counting instrument used for nanosecond fluorescence lifetime measurements.

femtosecond laser system (see Figure II-2). The apparatus was based on a mode-locked Ti:sapphire laser (Spectra-Physics, Tsunami; center wavelength 800 nm, pulse width ~70 fs, repetition rate 82 MHz) pumped by a CW green laser (Spectra-Physics, Millenia V; 532 nm, 4.5 W). The repetition frequency was reduced to 4 MHz by using a pulse picker (Spectra-Physics, model 3980), and the third harmonic (266 nm, FWHM ~250 fs) was used as the excitation source. The monitoring system consisted of a microchannel plate photomultiplier tube (MCP-PMT; Hamamatsu, R3809U-51) cooled to -20 °C and a single-photon counting module (Becker and Hickl, SPC-530). The fluorescence photon signal detected by the MCP-PMT and the photon signal of the second harmonic (400 nm) of the Ti:sapphire laser were used for the start and stop pulses of a time-to-amplitude converter in this system. The instrument response function had a half-width of about 25 ps. The fluorescence time profiles were analyzed by deconvolution with the instrument response function.

II-3   *Photoacoustic measurements*

The experimental setup for time-resolved photoacoustic (PA) measurements is shown in Figure II-3. PA measurements were made by using a Nd^{3+}:YAG laser (Spectra Physics, GCR-130, pulse width 6ns, 266nm) or a XeCl excimer laser (Lambda Physik, Lextra 50, pulse width 17 ns, 308 nm) as the excitation source. The sample solution was irradiated by the laser beam after passing through a slit (0.5 mm width). The effective acoustic transit time was estimated to be ca. 340 ns. The laser fluence was varied using a neutral density filter, and the laser pulse energy was measured with a pyroelectric energy meter (Laser Precision, RJP-753 and RJ7620).

Figure II-2 block diagram components:

- CW Green laser 532nm → Mode locked Ti:Sapphire laser 82MHz 800nm 70fs → Pulse picker SHG (second harmonic generator) 82MHz 4MHz → THG (Third harmonic generator) → PD
- 400nm Horizontal (200fs)
- 266nm vertical (250fs)
- MCP-PMT → MC
- CFD (constant fraction discriminator) — Start pulse / Stop pulse → TAC (time to amplitude converter) → PGA (programmable gain amplifier) → ADC (analog digital converter) → Memory

MCP-PMT: Microchannel plate PMT
PD: Photodiode, MC: Monochromator

Figure II-2. Block diagram of a picosecond time-resolved fluorometer based on the time-correlated single photon counting method.
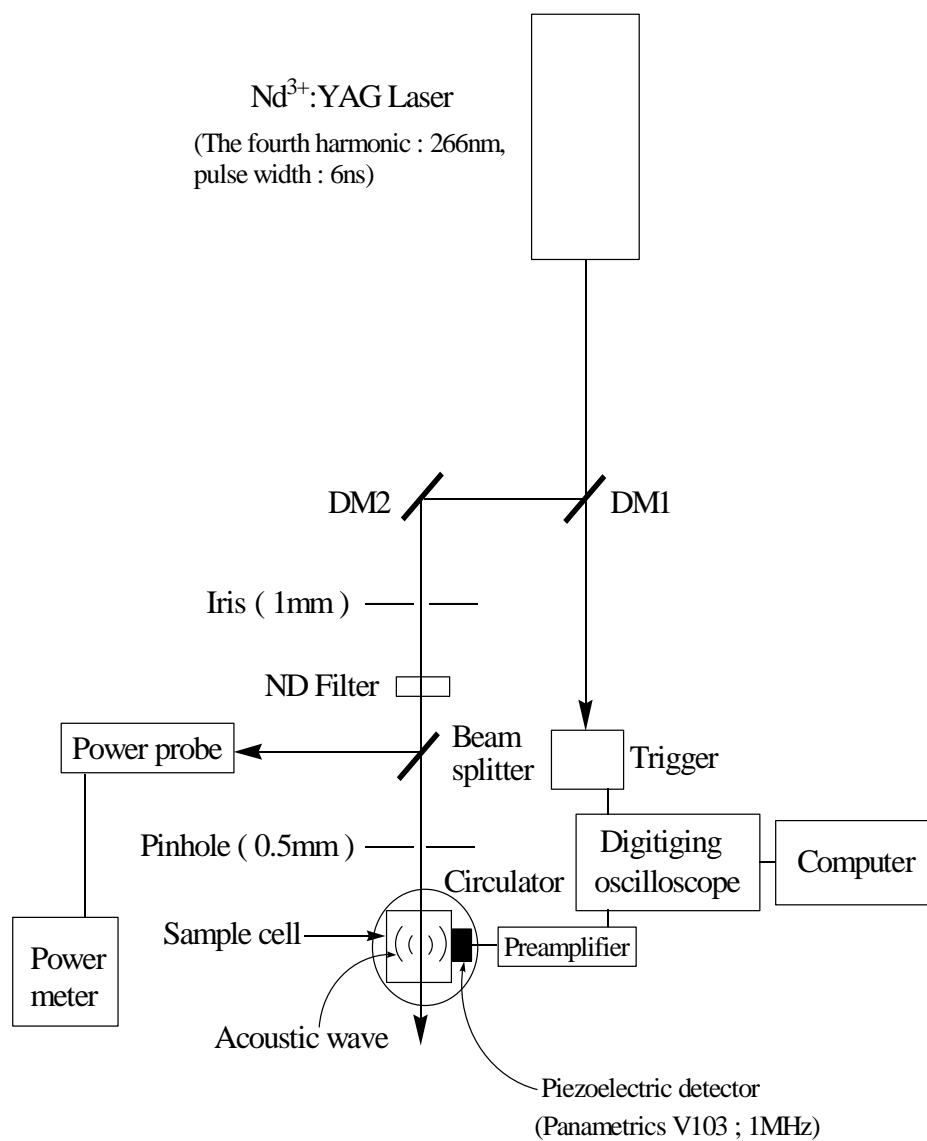
Figure II-3. Schematic diagram of time-resolved photoacoustic spectroscopy (PAS) system.

The PA signal detected by a piezoelectric detector (panametrics V103, 1 MHz) was amplified by using a wide-band high-input impedance amplifier (panametrics 5676, 50 kHz, 40 dB) and fed to a digitizing oscilloscope (Tektronix, TDS-744). The temperature of the sample solution was held to $\pm 0.02°C$.

The intensity (H) of photoacoustic signal can be expressed as

$$H = K\alpha(1-10^{-A})E_L \qquad\qquad (\text{II-2})$$

where K is a constant containing the thermoelastic properties of the solution and instrumental factors, E_L is the laser pulse fluence, A is the absorbance of the sample solution and α is the fraction of energy deposited in the medium as prompt heat within the time resolution of the experiment [3,4] (see Appendix A.). Figure II-4 shows the photoacoustic signals taken for 2-hydroxybenzophenone (2HBP) in CH_3CN at 293K. The signal amplitude plotted against laser fluence gave a straight line in Figure II-5. Since it is known that the α value for the reference compound (2HBP) can be assumed to be unity, one can determine the α value of the sample compound by calculating the ratio of the slopes of straight lines. Figure II-6 shows the plot of H/E_L vs. absorptivity, $(1-10^{-A})$ of 2HBP in CH_3CN at 293K. The absorptivity dependency shown in this figure is consistent with equation II-2.

Figure II-4. Laser fluence dependence of PA signals for 2HBP in CH_3CN (E_λ=266nm).
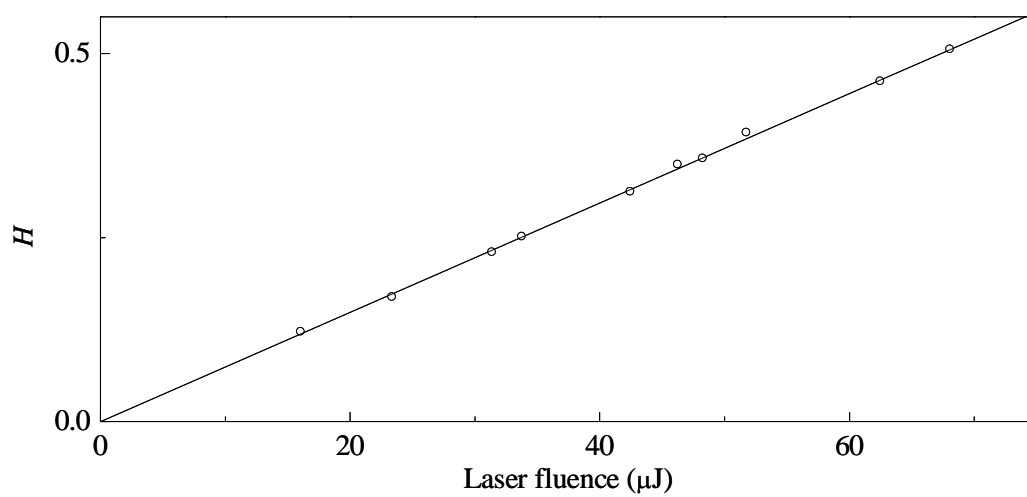
Figure II-5. PA signal amplitudes as a function of laser energy for 2HBP in CH_3CN (E_λ=266nm).
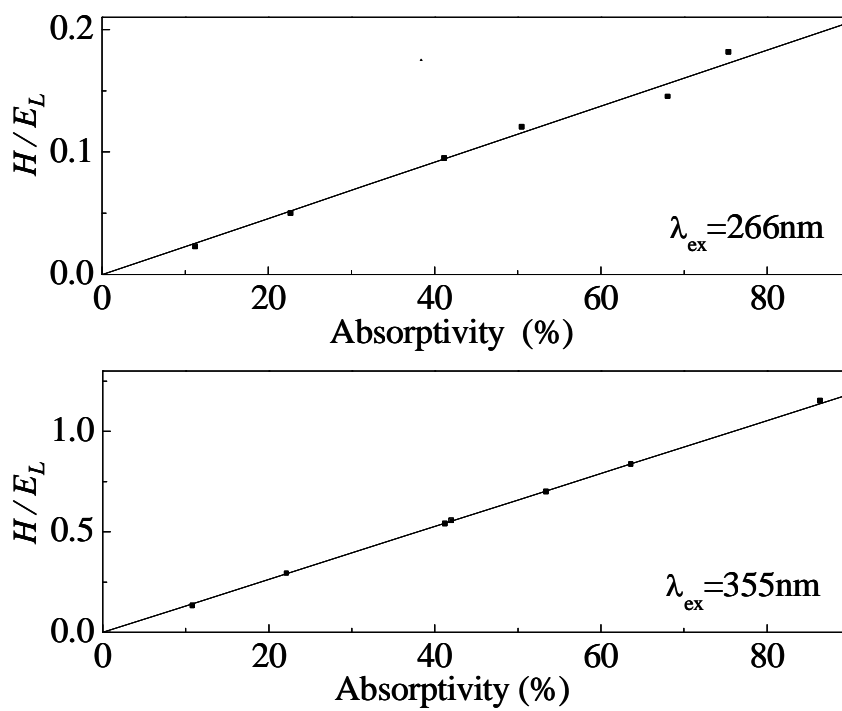
Figure II-6. Plot of H/E_L vs. absorptivity $(1-10^{-A})$ of 2HBP in CH_3CN at 293K
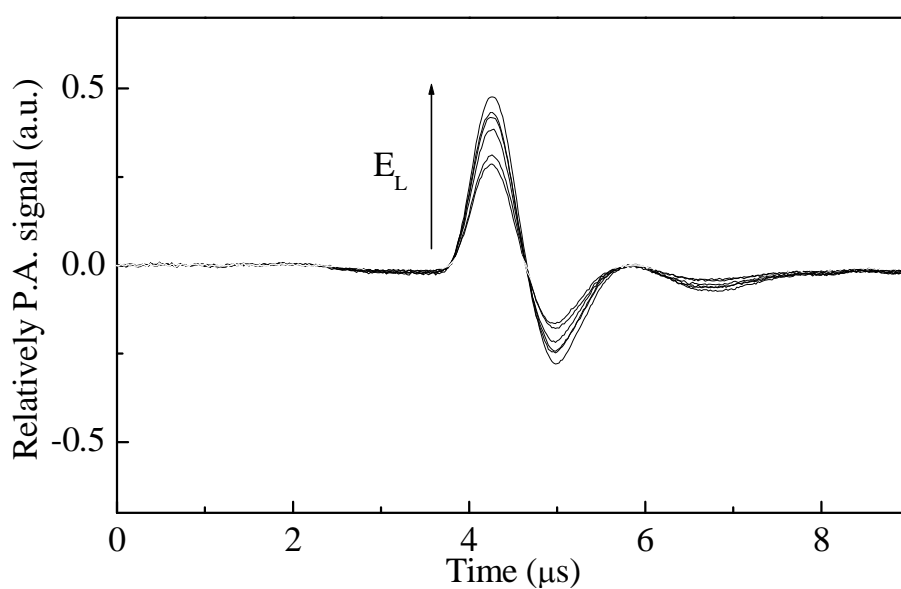
Appendix A.

Photoacoustic effects

The photoacoustic effect was first discovered by Alexander Graham Bell in his search for a means of wireless communication in 1880. Bell succeeded in transmitting sound with an invention he called the "photophone," which carried a vocal signal with a beam of sunlight that was reflected by a vocally modulated mirror. Additionally, the photoacoustic effect have applied in spectroscopy, Bell developed the "spectrophone," essentially an ordinary spectroscope equipped with a hearing tube instead of an eyepiece.

Samples could then be analyzed by sound when a source of light was applied, the spectrophone provided a means for measuring spectra beyond the visible regime that were previously undetectable. The light source, either pulsed or modulated, periodically heats the sample by the photothermal effect. Periodic sample heating followed by expansion causes a periodic pressure wave which is detected with the pressure transducer.

Theory

Photoacoustic spectroscopy is based on the absorption of light, leading to the local warming of the absorbing volume element. The subsequent expansion of the volume element generates a pressure wave proportional to the absorbed energy, which can be detected by pressure detectors.

Rothberg and co-workers [5] initially modeled the photoacoustic experiment with a point source of heat given the analytical form $(1/\tau)\exp(-t/\tau)$ where τ is the lifetime of the transient and the pre-exponential term $1/\tau$ is a normalization factor so that the total heat deposition of transient is independent of τ.

The pressure transducer signal reflects the original heat deposition profile in space and time. Local thermal expansion initiates acoustic waves that obey the wave equation

$$\nabla^2 P(r',t) - \frac{1}{v_s}\frac{\partial P(r',t)}{\partial t^2} = -4\pi h(r',t) \tag{II-1}$$

where $h(r',t)$ is heat source function where r' and t refer to the spatial and temporal source coordinate, v_s is the speed of sound in the (assumed to be dispersionless and linear) medium and $P(r',t)$ is the wave amplitude at the observer's coordinate r', t. Where $h(r',t)$ assume impulse source as the spread of the sound in spherical symmetry field, the wave amplitude at the detector is given by

$$P(r_0,t) = \frac{h_0}{4\pi r_0}\frac{1}{\tau}e^{-(t-r_0/v_s)/\tau} \tag{II-2}$$

where r_0 is the distance from heat source, h_0 is total heat deposition. A transducer converts $P(r_0,t)$ to an electrical signal. The transducer such as PZT was defined to be sensitive to longitudinal displacement waves and was modeled as an underdamped harmonic oscillator whose impulse response (i.e., Green's function).

$$G(t,t') = A\sin(v\,(t-t'))e^{-(t-t')/\tau_0} \tag{II-3}$$

Where $G(t,\,t')$ is Green's function for the transducer, v is the characteristic oscillation frequency of the transducer. The detector response $V(t)$ for an arbitrary forcing function $P(r_0,t)$ is given by convolving the impulse response with the forcing

function:

$$V(t) = \int_{-\infty}^{t} G(t, t') P(r_0, t') dt' \qquad \text{(II-4)}$$

Thus, the photoacoustic waveforms (time domain convolution of the heat source and detector) can be modeled according to the following equation

$$V(t) = \frac{h_0 A}{4\pi r_0} \frac{v/\tau}{v^2 + (1/\tau')^2} e^{-t/\tau} - e^{-t/\tau_0} [\cos(vt) - \frac{1}{v\tau'} \sin(vt)] \qquad \text{(II-5)}$$

where $V(t)$ is the detector response, $h_0 A/\pi r_0$ is constant, v is the characteristic oscillation frequency of the transducer (1MHz), τ_0 is relaxation time of the transducer, τ is the transient, and $1/\tau' = 1/\tau - 1/\tau_0$.

For n simultaneous reactions, $V(t)$ is given by [6]

$$V(t) = \sum_{k=1}^{n} K' \phi_k \frac{v/\tau_k}{v^2 + (1/\tau_k')^2} \left\{ e^{-t/\tau_k} - e^{-t/\tau_0} [\cos(vt) - \frac{1}{v\tau_k'} \sin(vt)] \right\} \qquad \text{(II-6)}$$

where K' is constant, ϕ_k is amplitude factor for transient k, ϕ_k is lifetime of transient k, and $1/\tau_k' = 1/\tau_k - 1/\tau_0$. Equation II-6 means that the observed acoustic wave resulting from the heat depositions of several simultaneous decays is the sum of the waveforms which would be observed from each of the decays individually.

Photoacoustic signal measurement

For photochemically simple systems with known quantum yield and kinetics, the amplitude of photoacoustic signal is related to the energy of the incident laser pulse

by [7]:

$$H = K\alpha(1-10^{-A})E_L \qquad \text{(II-7)}$$

where H is the experimentally obtained amplitude of the acoustic signal, K is instrumental constant which depends on the geometry of the experimental set-up and the thermoelastic quantities of the medium, E_L is the incident laser pulse energy, A is optical density of the solution, and α is the fraction of the absorbed laser energy released as thermal energy within the response time of the detector (prompt heat).

$$\alpha = E_{th}/E_{abs} \qquad \text{(II-8)}$$

where $0 \leq \alpha \leq 1$. The application of equation II-7 supposes a cylindrical acoustic wave.

H is used to determine the fraction of heat stored by species with τ_{nr} longer than the experimental time resolution of the instrument. In order to eliminate K, a calorimetric reference is needed. Using a calorimetric reference with $\alpha = 1$, the value of α for the sample is the ratio between H/E_L for sample and reference.

Heat integration time

The probable origin for this lower limit is that the measurements are ultimately limited by the acoustic transit time (τ_a) of the PAS apparatus. This parameter is defined as

$$\tau_a = R/V_a \qquad \text{(II-9)}$$

where τ_a is the time required by the acoustic wave to travel across the laser beam radius, R is the radius of the excitation beam and V_a is the velocity of sound in the sample medium. Assuming that the beam radius is 0.5 mm and a velocity of sound in water is 1470 m s^{-1} at 293K, the acoustic transit time becomes 340 ns.

References

[1] Grabner, G.; Köhler, G.; Zechner, J.; Getoff, N. *Photochem. Photobiol.* **1977**, *26*, 449.

[2] Perichet, R. G.; Chaperon, R.; Pouyet, B. *J. Photochem*. **1980**, *13*, 67.

[3] Braslavsky, S. E.; Heibel, G. E. *Chem. Rev*. **1992**, *92*, 1381.

[4] Braslavsky S. E.; Heihoff, K. In *Handbook of Organic Photochemistry*, Scaiano, J. C., Ed., CRC Press: Boca Raton, FL1989; Vol. 1, p327.

[5] Rothberg, L. J.; Simon, J. D.; Bernstein, M.; Peters, K. S.*; J. Am. Chem. Soc.* **1983**, *105*, 3464.

[6] Rudzki, J. E.; Goodman, J. L.; Peters, K. S. *J. Am. Chem. Soc.* **1985**, *107*, 7849.

[7] (a) Braslavsky, S. E.; Heibel, G. E. *Chem. Rev*. **1992**, *92*, 1381. (b) Churio, M. S.; Angermund, K. P.; Braslavsky, S. E. *J. Phys. Chem*. **1994**, *98*, 1776. (c) Gensch, T. ; Braslavsky, S. E. *J. Phys. Chem. B* **1997**, *101*, 101. (d) Small J. R. Libertini, L. J.; Small, E. W. *Biophys. Chem*. **1992**, *42*, 29. (e) Borsarelli, C. D.; Bertolotti, S. G.; Previtali, C. M *Photochem. Photobiol. Sci.* **2003**, *2*, 791.

Chapter III

Excited-State Proton Transfer Reaction of

Trifluoromethylphenols in Water

III -1 *Introduction*

Hydroxyarenes such as 1- and 2-naphthols are well known to undergo excited-state proton transfer (ESPT) to solvent in water because of drastic enhancement of the acidity in the first excited singlet (S_1) state [1]. The occurrence of ESPT is usually substantiated by appearance of dual fluorescence originating from the protonated and deprotonated species. In the case of phenol (PhOH) however, the extremely small fluorescence quantum yield ($\Phi_f = 8.0 \times 10^{-4}$ in water) and short lifetime ($\tau_f = 18$ ps) of the phenolate anion render difficult the direct observation of the proton transfer process in the excited state, and only a few papers can be found on ESPT reactions of phenols in the literature [2-4]. In this chapter, it will be described that the introduction of an electron-withdrawing trifluoromethyl (CF_3) group into the aromatic ring of PhOH enhances significantly the fluorescence quantum yield and lifetime of the deprotonated forms, and the fluorescence spectrum exhibits dual fluorescence due to the protonated and deprotonated forms (Scheme III-1). The acidity of PhOH is increased both in the ground and excited states by introducing a CF_3 group in the aromatic ring.
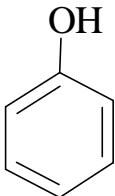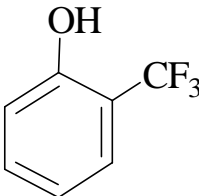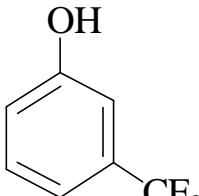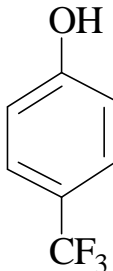
This chapter describes the first direct measurement of the rate of proton transfer to solvent from excited *o*-, *m*-, and *p*-TFOHs in water. The sample compounds and abbreviations are shown in Scheme III-2.

III-2 *Material*

Phenol (PhOH, Wako), *o*-trifluoromethylphenol (*o*-TFOH, WAKO) and *p*-trifluoromethylphenol (*p*-TFOH, WAKO) were purified by vacuum sublimation. *m*-trifluoromethylphenol (*m*-TFOH, Acros) was distilled under reduced pressure.
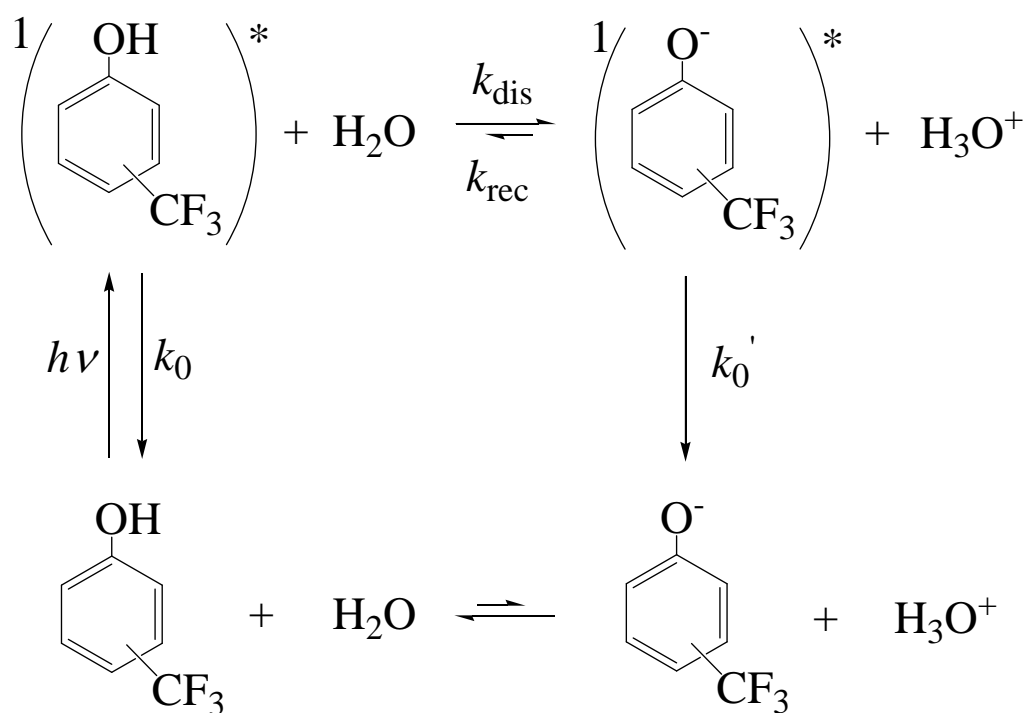
Scheme III-1. Kinetic scheme for prototropism of trifluoromethylphenol in aqueous solution.

	PhOH	o-TFOH	m-TFOH	p-TFOH
$pK_a{}^a$	9.99	8.25	8.95	8.68
$pK_a{}^{*a}$	3.6	1.1	1.5	~2

Scheme III-2. Structures and abbreviations of the sample compounds, pK_a values in the ground state, and those in the S_1 state ($pK_a{}^*$) estimated by the Förster cycle method. [a] From ref. 3.

Acetonitrile (CH$_3$CN, Kanto) was purified by distillation. Deionized water was purified by using a Millipore (MILLI-Q-Labo). D$_2$O (Merck, >99.8%) was used as received. H$_2$SO$_4$ (Wako, 97%, S. S. grade) or KOH (Kanto) was used to adjust the acid concentration of sample solutions. The pH value of sample solutions was determined by using a pH meter (Horiba, F-8).

III-3 *Spectral properties*

Figure III-1 shows the absorption and fluorescence spectra of PhOH, TFOHs (*o*-TFOH, *m*-TFOH and *p*-TFOH) in aqueous solutions and CH$_3$CN at room temperature. The ground state pK_a values of the TFOHs are reported as shown in Scheme III-2 [3]. The absorption spectra of PhOH, *o*-TFOH, *m*-TFOH, and *p*-TFOH in aqueous solution (pH 4.7) almost coincide with those in CH$_3$CN, showing that in aqueous solutions (pH 4.7), the ground-state proton dissociation does not occur in these compounds.

It is noteworthy that the fluorescence spectra of *o*- and *m*-TFOH in H$_2$O exhibit dual fluorescence bands: normal and large Stokes-shifted fluorescence bands with maxima at around 310 and 345nm, respectively. The fluorescence spectrum of *p*-TFOH in H$_2$O also shows a similar feature, although the intensity of the longer-wavelength band is much weaker than those of *o*- and *m*-TFOH, and both bands appear at shorter wavelengths. The shorter-wavelength bands of TFOHs resemble their fluorescence spectrum in CH$_3$CN, and the longer-wavelength bands almost coincide with the fluorescence spectrum of the deprotonated forms (anions) in H$_2$O. The excitation spectrum monitored at the longer- and shorter-wavelength bands agreed with the absorption spectrum. These indicate that both bands originate from the parent molecule and suggest the occurrence of ESPT to solvent.
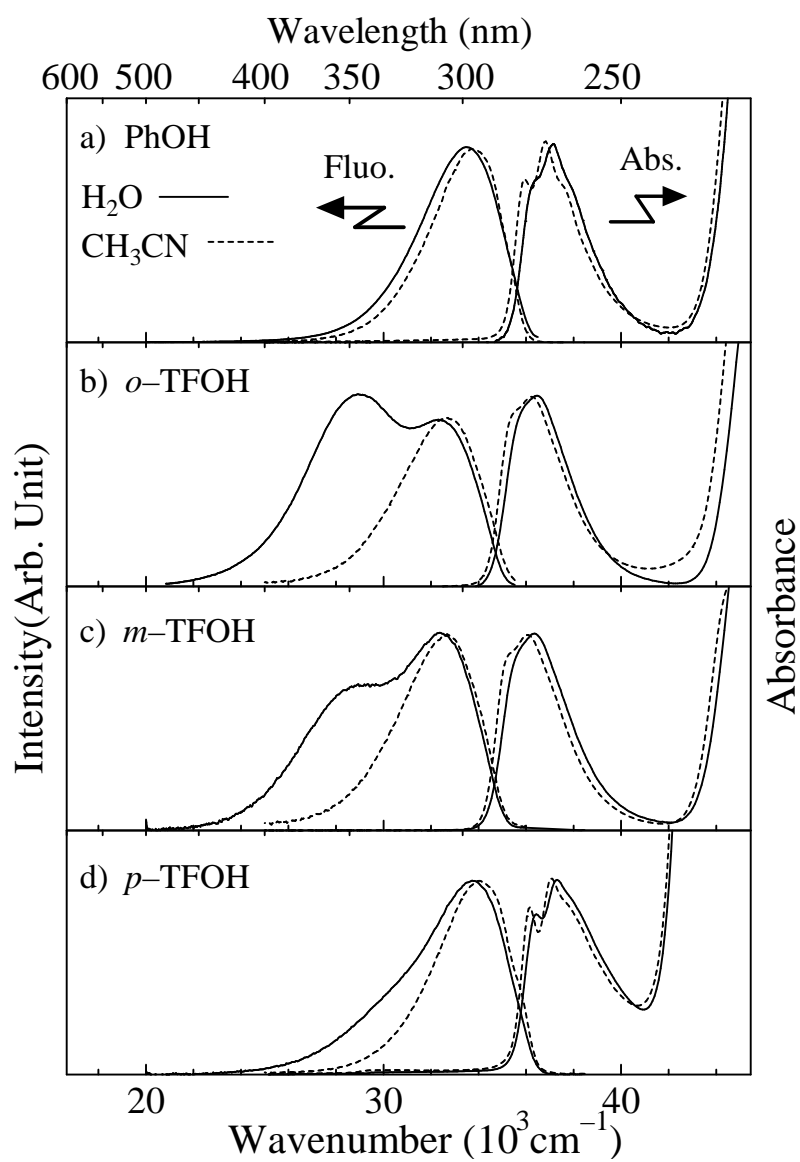
Figure III-1. Absorption and fluorescence spectra of (a) PhOH, (b) *o*-TFOH, (c) *m*-TFOH, (d) *p*-TFOH in H_2O (pH 4.7, solid line) and CH_3CN (broken line) at room temperature.

Table III-1 show fluorescence lifetimes of PhOH and TFOHs in H_2O and in organic solvents, cyclohexane (CH) and CH_3CN. The fluorescence lifetimes of TFOHs in H_2O are relatively shorter than those of TFOHs in organic solvents. Shorter lifetime of TFOHs in H_2O suggests the occurrence of the excited-state proton dissociation.

Figure III-2 illustrates the absorption and fluorescence spectra of PhOH, *o*-TFOH, *m*-TFOH, and *p*-TFOH in H_2O (pH = 4.7) and D_2O (pD = 4.7) at 293K. An interesting feature in Figure III-2 is remarkably large isotope effects on the fluorescence spectra; the longer-wavelength fluorescence bands of TFOH in H_2O almost disappear in TFOD in D_2O for all the isomers. This suggests significant decreases in the proton transfer rate by deuterium substitution.

III-4   *Rate of proton dissociation*

Since the decay time constant of the deprotonated anion TFO^{-*} shown as Table III-2 is relatively short (260, 450, and 290 ps for *o*-, *m*-, and *p*-TFO^-, respectively), the excited-state protonation reaction ($k_{rec}[H_3O^+]$ in Scheme III-1) can be neglected under moderately acidic conditions ($[H_3O^+] < 10^{-4}M$) [5]. The fluorescence kinetics of $^1TFOH^*$ and $^1TFO^{-*}$ on excitation by a δ-pulse follows the monoexponential and biexponential laws, respectively:

$$I_f^{TFOH}\left(t\right) = A_0\, e^{-(k_0+k_{dis})t} \tag{III-1}$$

$$I_f^{TFO^-}\left(t\right) = A_0{'}\left[e^{-(k_0+k_{dis})t} - e^{-k_0{'}t} \right] \tag{III-2}$$

Table III-1   Fluorescence lifetime of phenol
derivatives in several solvents at 298K.

|	τ_f (ns)		
	H$_2$O	CH	CH$_3$CN
PhOH	3.1	2.4	6.4
o-TFOH	0.36	2.4	2.5
m-TFOH	0.74	2.7	2.3
p-TFOH	1.7	3.9	3.1
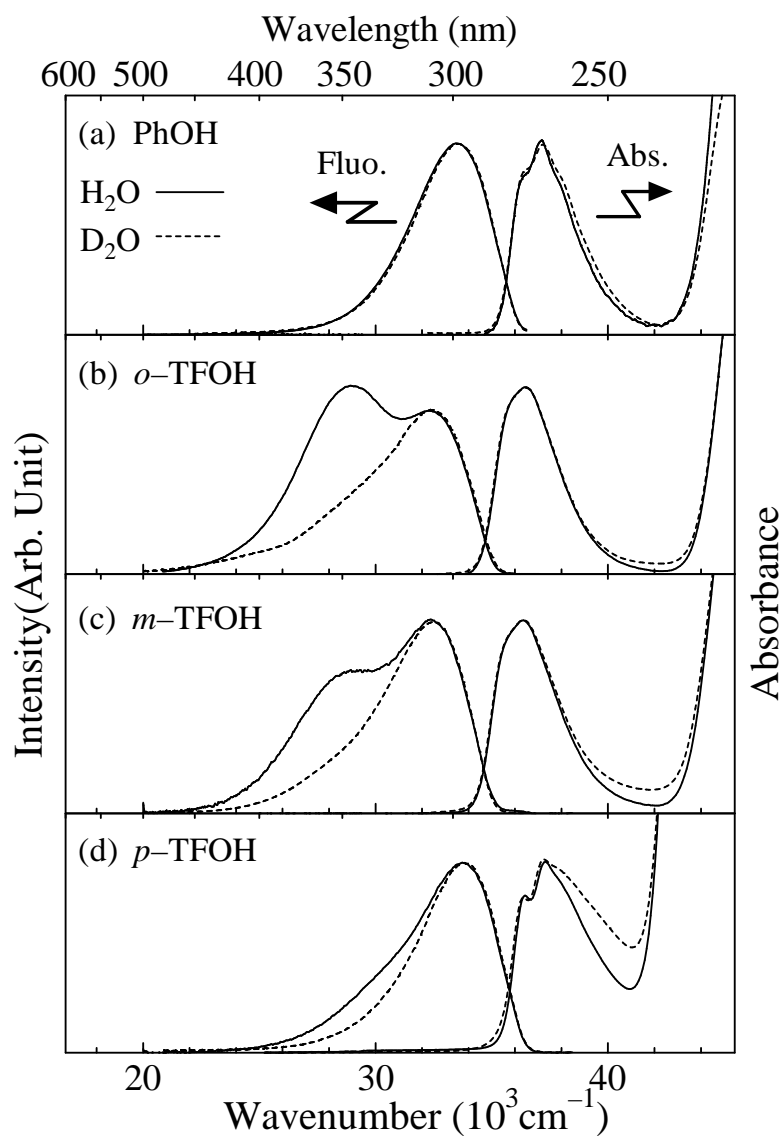
Figure Ⅲ-2. Absorption and fluorescence spectra of (a) PhOH, (b) *o*-TFOH, (c) *m*-TFOH, and (d) *p*-TFOH in H_2O (pH 4.7, solid line) and D_2O (pD 4.7, broken line) at room temperature.

Table III-2   Fluorescence lifetime (τ_f) and fluorescence quantum yield (Φ_f) of TFO⁻s formed by indirect excitation from neutral via ESPT reaction in H_2O.

	Φ_f	τ_f (ps)
o-TFO⁻	2.1×10^{-2}	260
m-TFO⁻	2.8×10^{-2}	450
p-TFO⁻	7.1×10^{-3}	290

In order to determine the proton dissociation rate constant (k_{dis}) of ^{1}TFOHs*, the fluorescence time profiles of o-TFOH, m-TFOH and p-TFOH and their anions (o-TFO$^-$, m-TFO$^-$ and p-TFO$^-$) in H_2O were taken as shown in Figure III-3, III-4, III-5, respectively. In Figures III-3 ~ III-5, the fluorescence time profiles of the shorter-wavelength band (monitored at 300 nm) and the longer-wavelength band (monitored at 360 nm) of o-TFOH are displayed along with the least-squares fitting curves determined based on equations III-1 and III-2. The solid lines represent the deconvoluted best fit of (a) a single exponential function (τ_{decay} = 360 ps) and (b) a two-exponential function (τ_{rise} = 240 ps and τ_{decay} = 360 ps) superimposed on the experimental data points. The rise time (240 ps) of the time profile in Figure III-3 (b) is in fair agreement with the lifetime of the deprotonated anion (260 ps). This demonstrates that the reaction sequence from TFOH* to TFO$^-$ (see Scheme III-1) follows a consecutive reaction with the rate constants k_{dis} and k_0' (($k_0 + k_{dis}$) < k_0'). Since the decay rate (τ_{decay}) of ^{1}TFOHs* corresponds to ($k_0 + k_{dis}$), the magnitude of k_{dis} can be estimated from (τ_{decay}^{-1} - τ_0^{-1}). It is assumed that τ_0 (= $1/k_0$) is equal to the fluorescence lifetime of TFOHs in CH_3CN where no dissociation occurs [6]. From the above kinetic analyses the rate constants for the proton dissociation reaction of o-, m-, and p-TFOH were obtained to be 2.2 x 10^9 s^{-1}, 8.6 x 10^8 s^{-1}, and 2.5 x 10^8 s^{-1}, respectively, at 293 K. The k_{dis} values of o- and m-TFOHs are much larger than that of PhOH which can be evaluated to be less than 2.0 x 10^8 s^{-1} from the fluorescence lifetime in H_2O (3.1 ns) and CH_3CN (6.4 ns) shown as Table III-3. The enhancement of the ESPT rate in TFOHs can be attributed to the electron-withdrawing effect of the CF_3 group. The electronic effects of substituents are composed of two main parts: a field/inductive component and a resonance component [7]. In the ESPT of TFOHs, the CF_3 group is anticipated to accelerate the proton dissociation rate by the

Figure III-3. Fluorescence time profiles of *o*-TFOH in H_2O at 298 K monitored at (a) 300 nm and (b) 360 nm ($\lambda_{exc} = 266$ nm). The instrument response function is denoted by broken line.
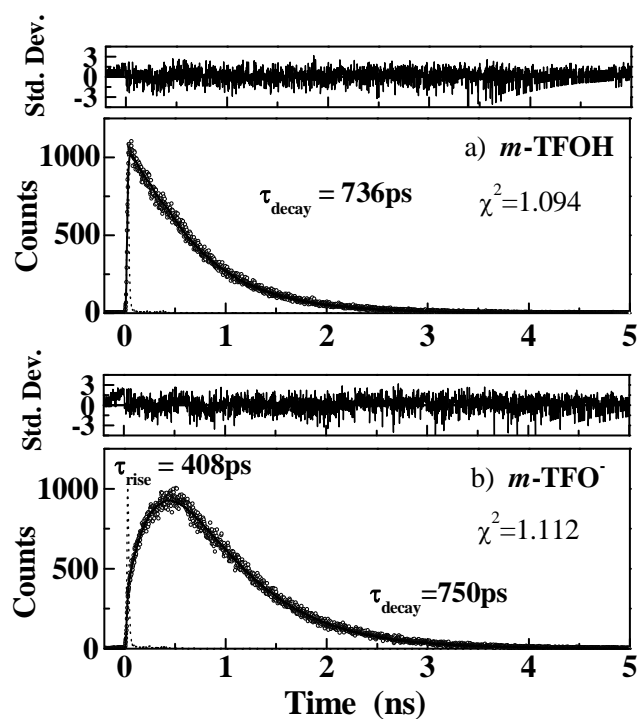
Figure III-4. Fluorescence time profiles of *m*-TFOH in H_2O at 298 K monitored at (a) 300 nm and (b) 360 nm (λ_{exc}=266nm). The instrument response function is denoted by broken line.
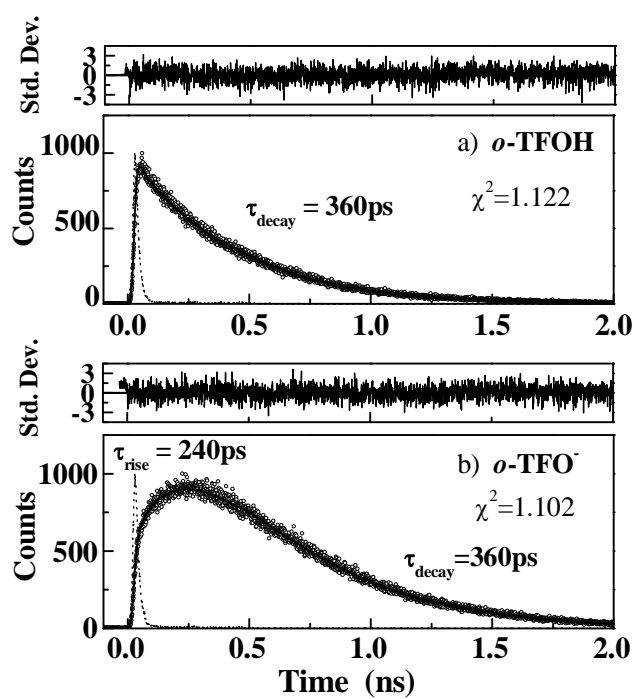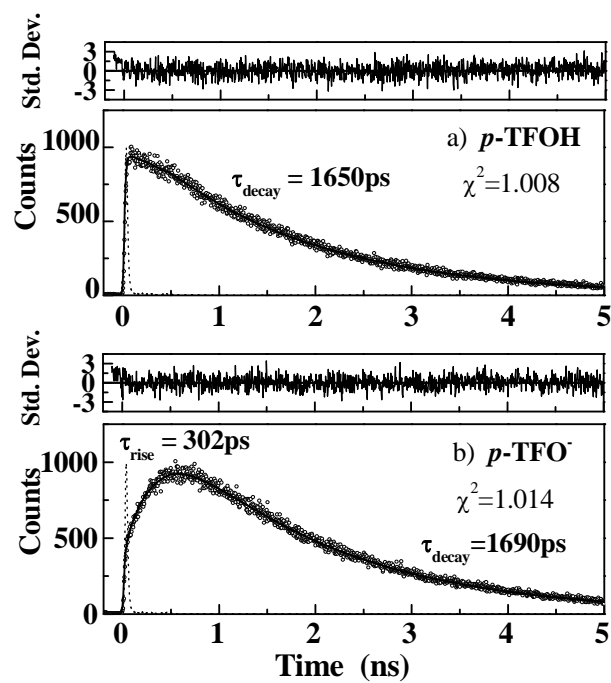
Figure III-5. Fluorescence time profiles of *p*-TFOH in H_2O at 298 K monitored at (a) 300 nm and (b) 360 nm (λ_{exc} = 266 nm). The instrument response function is denoted by broken line.

inductive effect acting through the intervening σ bonds. According to Hynes et al [8], the differences in ground-state acidity among several substituted phenols are due mainly to effects in the phenolate anions, the effects in the corresponding phenols being of minor importance. Our results reveal that a similar effect of the CF_3 group is also applicable for the excited-state acidity of TFOHs.

III-5   *Activation energy of the excited-state proton dissociation*

The Arrhenius plot of the k_{dis} values of TFOHs in H_2O and D_2O gave straight lines in the temperature range between 278 and 323K (see Figure III-6). The activation energy and the frequency factor for the excited-state proton dissociation reaction were obtained as shown in Table III-3. Although the magnitude of the frequency factor is nearly constant among TFOHs, the activation energy of *o*-, *m*-, and *p*-TFOH increases in that order, and all TFOHs show larger E_a values in D_2O than in H_2O. The ESPT rates ($\sim 10^8 - 10^9$ s^{-1}) of TFOHs at the temperature range between 275 and 323K are significantly slower than that ($\sim 10^{11}$ s^{-1}) of the solvent relaxation rate of water [9]. These indicate that at the above temperature range, the solvent relaxation is sufficiently fast and the rate-determining step in the ESPT reaction is the actual proton-transfer step. The activation energy and the deuterium isotope effect ($k_{dis}^H/k_{dis}^D = 3.0$–$6.0$) are ascribed to the proton motion along the proton-transfer coordinate. Figure III-7 shows temperature function of the isotope effect (k_{dis}^H/k_{dis}^D) of TFOHs in H_2O (pH 4.7) and D_2O (pD 4.7). The isotope effect of *p*-TFOH depends on temperature more strongly than that of *o*-TFOH and *m*-TFOH.

III-6 *Conclusion*

The proton transfer reactions to solvent from electronically excited *o*-, *m*-, and *p*-trifluoromethylphenols (TFOHs) in water have been investigated by picosecond time-resolved fluorescence measurements. The rate constants for the proton dissociation of *o*-, *m*-, and *p*-TFOH are obtained to be 2.2 x 10^9, 8.6 x 10^8, and 2.5 x 10^8 s^{-1}, respectively. On the basis of the rate constants, the effects of substituent and deuterium isotope effects on the proton transfer reactions are revealed.
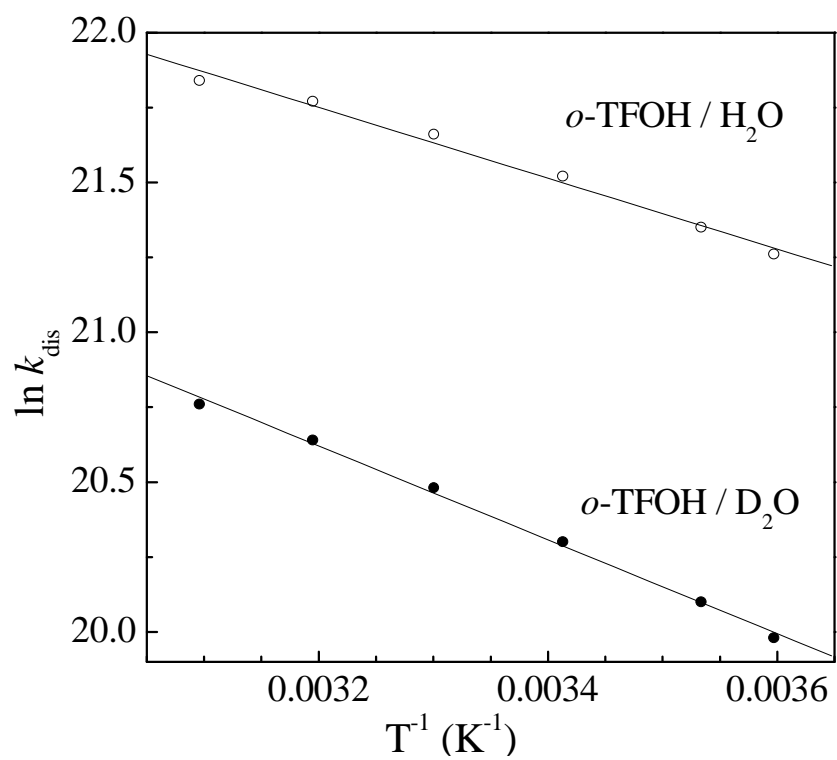
Figure. III-6. Arrhenius plots of the proton-dissociation rate constant (k_{dis}) of *o*-TFOH in H_2O and D_2O (pD4.7).

Table III-3. Proton dissociation rate (k_{dis}) and isotope effect (k_{dis}^H/ k_{dis}^D) at 293 K, activation energy (E_a), and frequency factor (A) for excited-state proton transfer reactions of TFOHs in H_2O (pH 4.7) and D_2O (pD 4.7).

compound	solvent	k_{dis} (10^8s^{-1})	E_a (kJmol^{-1})	A (10^{11}s^{-1})	$\dfrac{k_{dis}^H}{k_{dis}^D}$
o-TFOH	H_2O	22	9.8	1.2	
	D_2O	6.6	13	1.4	3.3
m-TFOH	H_2O	8.6	12	1.1	
	D_2O	2.2	15	1.2	3.9
p-TFOH	H_2O	2.5	14	0.87	
	D_2O	0.44	21	2.9	5.7

Figure III-7. Temperature function of the isotope effect (k_{dis}^{H}/k_{dis}^{D}) of TFOHs in H_2O (pH 4.7) and D_2O (pD 4.7).

References

[1] Agmon, N.; *J. Phys. Chem. A* **2005**, *109*, 13.

[2] Wehry, E. L.; Rogers, L. B. *J. Am. Chem. Soc.* **1965**, *87*, 4234.

[3] Seiler, P.; Wirz, J. *Helv. Chim. Acta*, **1972**, *55*, 2693.

[4] Schulman, S. G.; Vincent, W. R.; Underberg, W. J. M. *J. Phys. Chem.* **1981**, *85*, 4068.

[5] Shiobara, S.; Tajima, S.; Tobita, S. *Chem. Phys. Lett.* **2003**, *380*, 673.

[6] Solntsev, K. M.; Huppert, D.; Agmon, N. *Phys. Rev. Lett.* **2001**, *86*, 3427.

[7] Hansch, C.; Leo, A.; Taft, W. *Chem. Rev.* **1991**, *91*, 165.

[8] a) Granucci, G.; Hynes, J. T.; Millie, P.; Tran-Thi, T.-H. *J. Am. Chem. Soc.* **2000**, *122*, 12243. b) Hynes, J. T.; Tran-Thi, T.-H.; Granucci, G. *J. Photochem. Photobiol. A* **2002**, *154*, 3.

[9] a) Rønne, C.; Åstrand, P.-O.; Keiding, S. R. *Phys. Rev. Lett.* **1999**, *82*, 2888. b) Rønne, C.; Keiding, S. R.; *J. Mol. Liquids* **2002**, *101*, 199.

Chapter IV

Excited-State Proton Transfer Reaction of

Cyanophenols in Water

IV-1   *Introduction*

Since the original works of Förster [1] and Weller [2], the excited-state proton transfer (ESPT) reactions of hydroxyaromatic molecules have been extensively investigated with particular interest on molecular mechanisms of proton transfer reactions in solution [3-11]. Until recently, a number of experimental and theoretical studies were carried out for 1- and 2-naphthols as prototypes of hydroxyaromatic molecules. Their proton dissociation rate constants in water at 298 K were directly determined by time-resolved fluorescence measurements to be 2.5 x 10^{10} and 1.1 x $10^8 s^{-1}$, respectively [12,13]. Robinson et al. [12,14] have suggested that the basic rate of weak photoacids, such as 1- and 2-naphthols, is limited by rotational reorientation of water molecules, and therefore, weak acid dissociation in water cannot take place on time scales shorter than the Debye rotational correlation time. Huppert and collaborators [15-18] have made comprehensive studies on the reversible proton dissociation and recombination of naphthol derivatives. Recently, Agmon has reported a very detailed description of ESPT reactions of naphthols on the basis of experimental and also theoretical studies [10].

This wealth of information available on the ESPT reaction of naphthols in aqueous solution is contrasted by the absence of similar data on phenol (PhOH) and its derivatives. Wehry and Rogers [19] investigated the influence of substituents upon the ESPT equilibrium constant (pK_a*) of a series of monosubstituted phenols. They found that the excited-state acidities can be correlated well with ground-state substituent constants evaluated by the Hammett and Taft equations and that conjugative effects are much more important, relative to inductive effects, in the excited states than in the ground state. Schulman et al. [20] investigated the

53

prototropic dissociation and reprotonation in the S_1 state of *o*-, *m*-, and *p*-cyanophenols (CNOHs) by steady-state and time-resolved fluorescence measurements. They estimated the rate constants for the proton dissociation of *o*-, *m*-, and *p*-CNOH to be 4.0 x 10^8, 1.9 x 10^8 and 2.8 x 10^7 s^{-1}, respectively. Because the fluorescence decay times of CNOHs are in a picosecond time range, the time resolution (~1.7 ns) of their apparatus used for the lifetime measurements might not be sufficient to obtain the accurate proton dissociation rates. In spite of the recent development of ultrafast laser spectroscopy, there seems to be few reports on the ESPT dynamics of PhOH and CNOHs in aqueous solution. The extremely weak fluorescence intensity of the deprotonated anion of phenols seems to render direct measurement of ESPT difficult. This is in contrast with 1- and 2-naphthols that exhibit strong fluorescence from the deprotonated form.

Phenol is an important constituent of the chromophore (*p*-hydroxybenzylidene-imidazolidinone) of green fluorescent protein (GFP) which is now widely used as noninvasive, genetically encoded reporters in biochemistry and cell biology [21,22]. It has been suggested that, in wild-type GFP (wtGFP), not only the deprotonated form of the chromophore but also the protonated form, which exhibits an absorption peak at 398 nm, gives the characteristic green emission resulting from the ESPT reaction to water molecules in the vicinity of the chromophore in GFP [23-26]. The tyrosine residue in proteins also possesses a phenol moiety as chromophore. The understanding of the ESPT reactions of phenol and its derivatives is, therefore, of great importance in biological studies as well as from fundamental aspects of proton transfer reactions.

In this chapter, the ESPT to solvent of PhOH and CNOHs (see Figure IV-1) is investigated by time-resolved fluorescence and photoacoustic (PA) measurements.

The ground-state pK_a values and those of the excited singlet (S_1) state (pK_a^*) are shown in Figure IV-1. The prototropic equilibrium of PhOH and CNOHs in the ground and S_1 states is depicted in Figure IV-2 along with the fluorescence and nonradiative deactivation processes from each excited species. This study was undertaken to answer the following questions: whether or not the ESPT to solvent occurs for PhOH and CNOHs in water, and, if it takes place, how fast are the rates and what factors determine the rate.

IV-2 *Material*

Phenol (PhOH, Wako), *o*-cyanophenol (*o*-CNOH, Tokyo Kasei), *m*-cyanophenol (*m*-CNOH, JANSSEN CHEMICA), and *p*-cyanophenol (*p*-CNOH, Aldrich) were purified by vacuum sublimation. Their methoxy analogues, *o*-methoxybenzonitrile (*o*-CNOCH$_3$, Aldrich), *m*-methoxybenzonitrile (*m*-CNOCH$_3$, AVOCADO), and *p*-methoxybenzonitrile (*p*-CNOCH$_3$, Aldrich) were used without further purification, except for anisole (PhOCH$_3$, Wako) which was distilled under reduced pressure. Sodium dichromate (Na$_2$Cr$_2$O$_7$, Kanto) was used as received. Acetonitrile (Kanto) was purified by distillation. Cyclohexane (CH, Aldrich, spectrophotometric grade), ethanol (Kishida, spectroscopic grade) and methanol (Kishida, spectroscopic grade) were used as received. Deionized water was purified by using a Millipore (MILLI-Q-Labo). D$_2$O (Merck, > 99.8%) was used as received. H$_2$SO$_4$ (Wako, 97%, S. S. grade) or KOH (Kanto) was used to adjust the acid concentration of sample solutions.
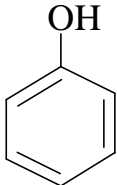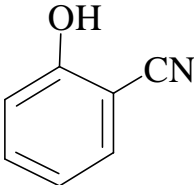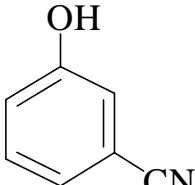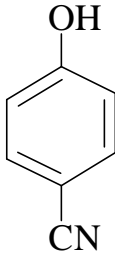
	PhOH	o-CNOH	m-CNOH	p-CNOH
pK_a	10.00^a	6.97^b	8.34^b	7.74^b
pK_a^*	3.0	-0.5	1.0	3.2

Figure IV-1. Structures and abbreviations of the sample compounds, pK_a values in the ground state, and those in the S_1 state (pK_a^*) estimated by the Förster cycle method. [a] From ref 19. [b] From ref 20

$$\text{ROH}^* + \text{H}_2\text{O} \underset{k_{\text{rec}}}{\overset{k_{\text{dis}}}{\rightleftharpoons}} (\text{RO}^{-*}...\text{H}_3\text{O}^+) \overset{\text{diffusion}}{\longleftrightarrow} \text{RO}^{-*} + \text{H}_3\text{O}^+$$

$h\nu \quad k_{\text{f}} \quad k_{\text{nr}} \qquad\qquad k_{\text{f}}{}' \quad k_{\text{nr}}{}' \qquad\qquad k_{\text{f}}{}'' \quad k_{\text{nr}}{}''$

$$\text{ROH} + \text{H}_2\text{O} \xleftarrow{1-\eta} (\text{RO}^-...\text{H}_3\text{O}^+) \xrightarrow{\eta} \text{RO}^- + \text{H}_3\text{O}^+$$
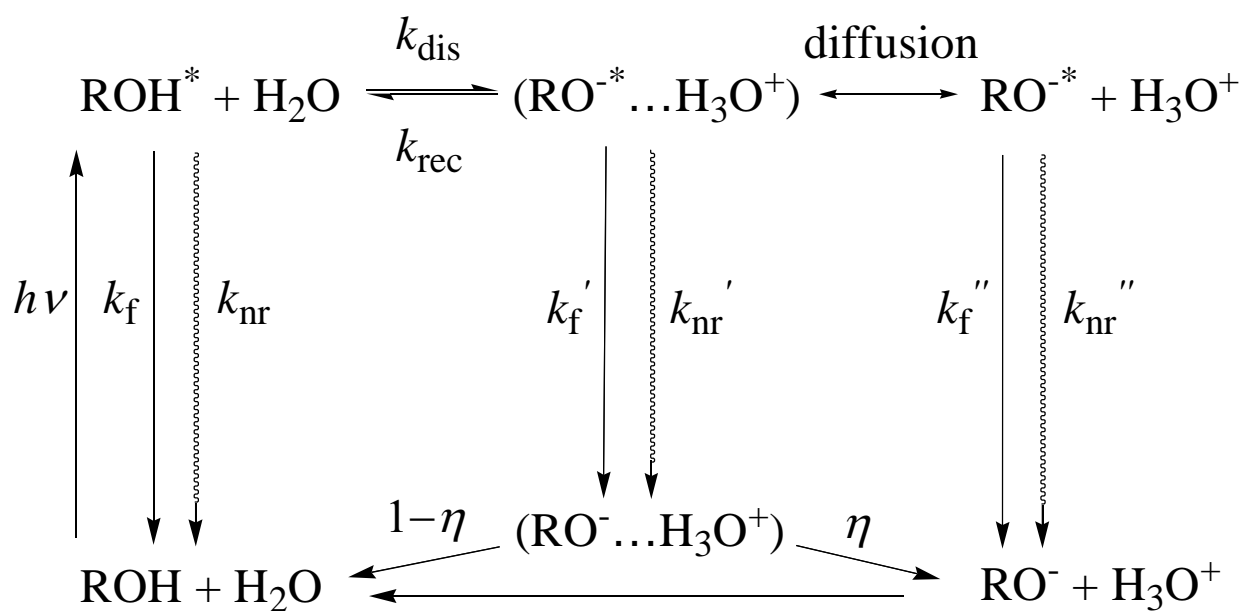
Figure IV-2. Kinetic scheme for prototropism of phenols in aqueous solution.

IV-3   *Spectral properties of phenol and cyanophenols*

Figure IV-3 shows the absorption and fluorescence spectra of PhOH, CNOHs (o-CNOH, m-CNOH, and p-CNOH), and their methoxy analogues (PhOCH$_3$; o-CNOCH$_3$, m-CNOCH$_3$, and p-CNOCH$_3$) at room temperature. The absorption spectra of PhOH and three CNOHs are little affected by the replacement of the hydroxyl group to the methoxy group. This shows that the electronic structures of PhOH and CNOHs are not altered significantly by the methoxy substitution. The fluorescence spectra of PhOH, m-CNOH, and p-CNOH almost coincide with those of their methoxy derivatives, except that the fluorescence spectra of the hydroxyl compounds are slightly red-shifted, probably because of hydrogen-bonding interactions with solvent molecules.

In contrast to the fluorescence spectra of PhOH, m-CNOH, and p-CNOH, o-CNOH exhibits dual fluorescence bands: normal and large Stokes-shifted fluorescence bands with maxima at 330 and 380 nm. The shorter-wavelength band resembles the fluorescence spectrum of the methoxy analogue. The excitation spectrum of the longer- and shorter-wavelength bands agreed with the absorption spectrum, indicating that both bands originate from the parent molecule. In the following discussions, it will be shown that the longer-wavelength band is due to the excited deprotonated form of o-CNOH which was produced by ESPT to solvent.
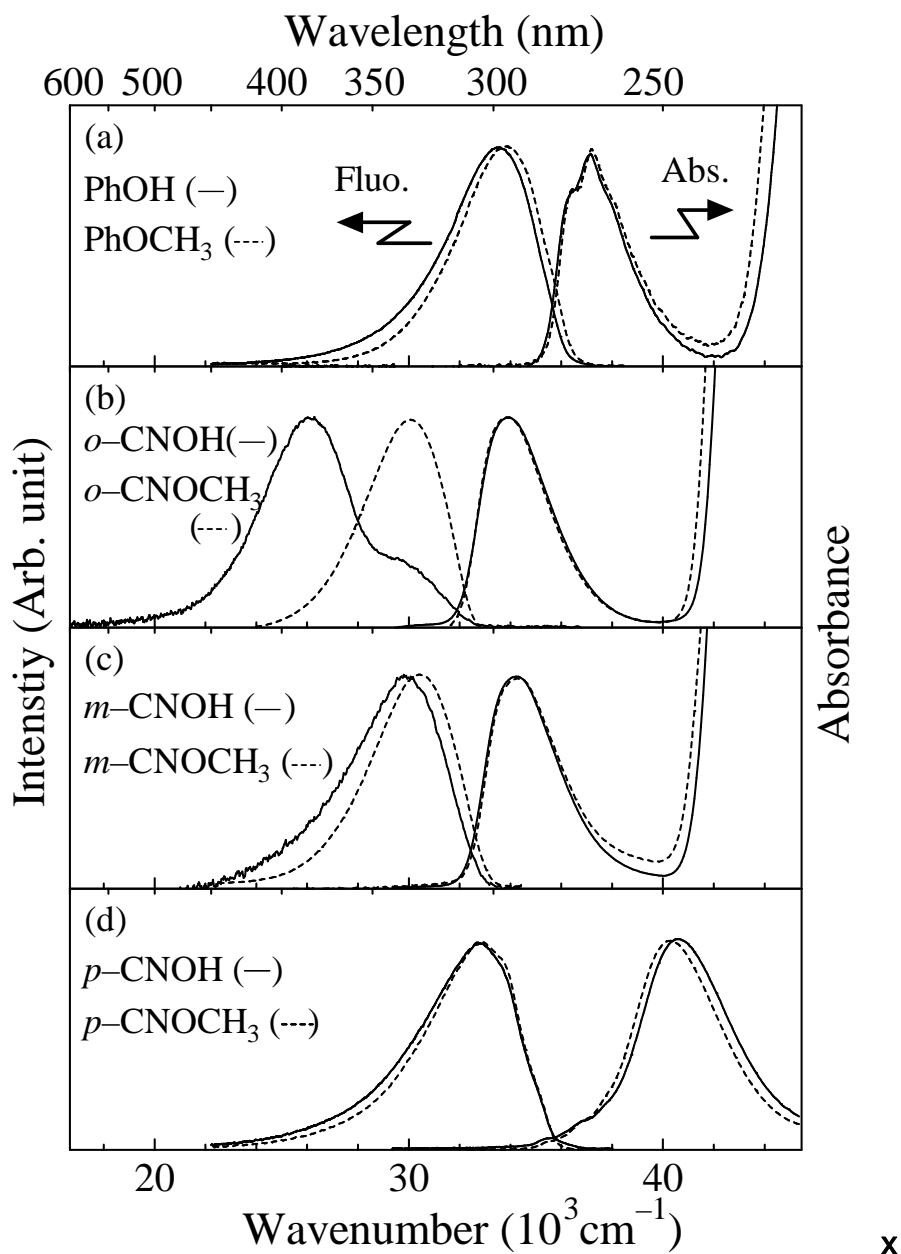
Figure IV-3. Absorption and fluorescence spectra of (a) PhOH (λ_{exc} = 250 nm) and PhOCH$_3$ (λ_{exc} = 250 nm), (b) *o*-CNOH (pH 4.0, λ_{exc} = 235 nm) and *o*-CNOCH$_3$ (λ_{exc} = 260 nm), (c) *m*-CNOH (λ_{exc} = 240 nm) and *m*-CNOCH$_3$ (λ_{exc} = 260 nm), (d) *p*-CNOH (λ_{exc} = 250 nm) and *p*-CNOCH$_3$ (λ_{exc} = 250 nm) in H$_2$O at room temperature. The pH adjustment of the sample solutions was not made except for *o*-CNOH (pH 4.0).

Figure IV-4 shows the absorption and fluorescence spectra of PhOH, CNOHs, and their deprotonated anions in aqueous solutions. The absorption and fluorescence spectra of the anions appear at much longer wavelengths compared with those of the protonated forms. It is noteworthy that the longer-wavelength band of o-CNOH is in fair agreement with the fluorescence spectrum of its anion. This also supports that in o-CNOH proton transfer to solvent takes place in the excited state.

As shown in Table IV-1, the fluorescence quantum yield (Φ_f) and lifetime (τ_f) of phenolate and cyanophenolate anions in water are extremely small, indicating that these excited anions undergo very rapid nonradiative deactivation from the S_1 state. This is in marked contrast to much larger Φ_f values of 1- and 2-naphtholate anions (0.12 and 0.57, respectively, in H_2O) [30]. On the basis of MO calculations, Wang et al. [31] have reported that the almost nonfluorescent property of phenolate anion can be ascribed to the electronically forbidden nature of the $S_1 \leftarrow S_0$ transition of the phenolate anion which belongs to the C_{2v} point group. However, the extremely short fluorescence lifetimes of the phenolate anion and its cyano derivatives demonstrate that very rapid nonradiative processes are involved in these anions in water. The nonradiative process is attributable, at least partly, to photoinduced electron ejection, although the quatum yield for the electron ejection is reported to be less than 0.2, even for the phenolate anion [32]. If the nonradiative deactivation is mainly due to the electron ejection from the fluorescent state, the cyano derivatives are expected to give longer lifetimes because of electron withdrawing effects of the cyano group. The actual lifetimes show an opposite tendency (see Table IV-1). The deuterium isotope effects observed for the fluorescence lifetime and remarkable enhancement of the lifetimes in CH_3OH and C_2H_5OH suggest that the rapid
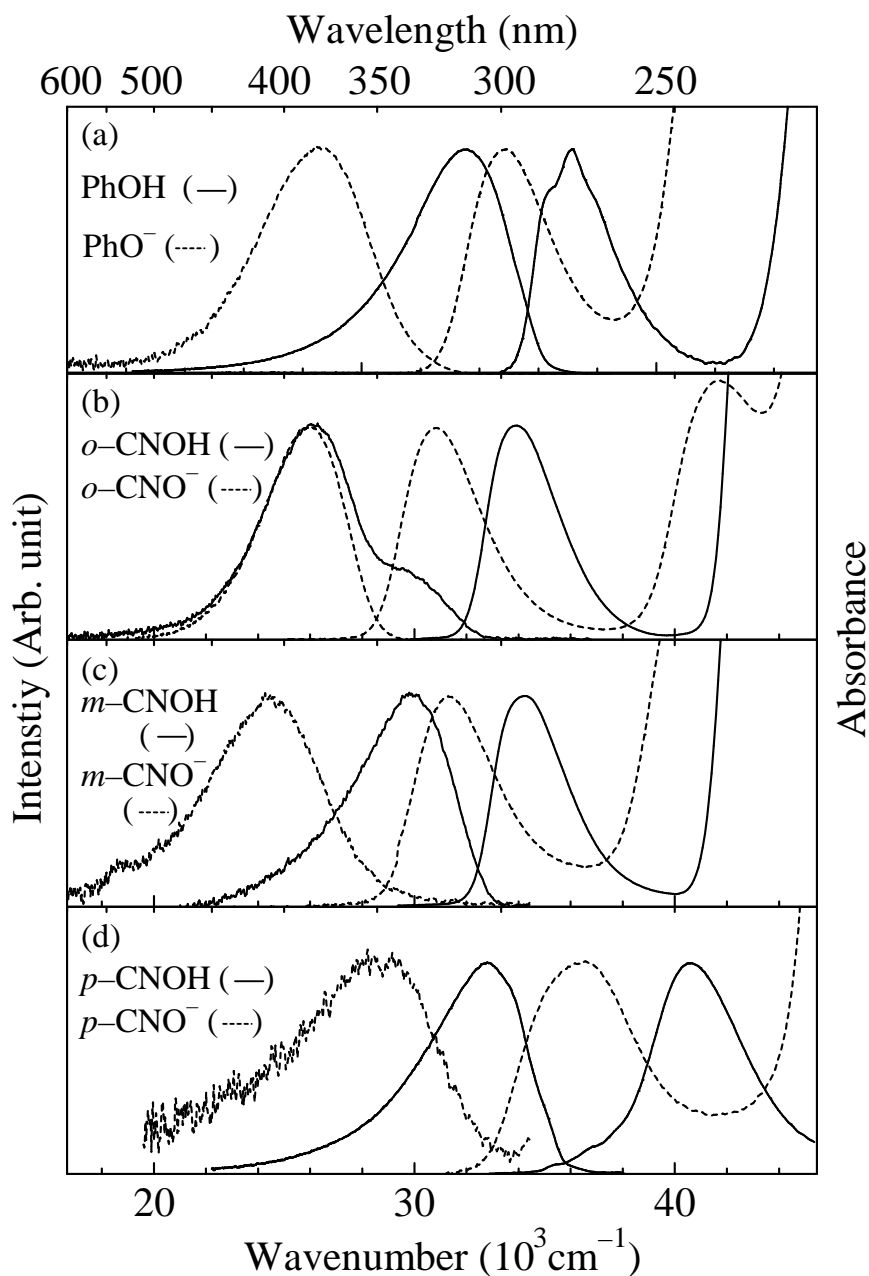
Figure IV-4. Absorption and fluorescence spectra of (a) PhOH (λ_{exc} = 250 nm) and PhO$^-$ (λ_{exc} = 250 nm),   (b) o-CNOH (pH 4.0, λ_{exc} = 235 nm) and o-CNO$^-$ (λ_{exc} = 250 nm), (c) m-CNOH (λ_{exc} = 240 nm) and m-CNO$^-$ (λ_{exc} = 240 nm), (d) p-CNOH (λ_{exc} = 250 nm) and p-CNO$^-$ (λ_{exc} = 260 nm) in H$_2$O at room temperature. The pH adjustment of the sample solutions is not made except o-CNOH (pH 4.0) and all the anions (pH 13).

61

Table IV-1: Fluorescence Quantum Yield (Φ_f) and Lifetime (τ_f) of Phenolate Anion and Cyanophenolate Anions in H_2O, D_2O, CH_3OH, and C_2H_5OH at 298 K

compound	Φ_f	τ_f (ps)			
	H_2O^a	H_2O^a	D_2O^b	CH_3OH^c	$C_2H_5OH^c$
PhO⁻	8.0×10^{-4}	18	43	345	477
o-CNO⁻	1.0×10^{-3}	30	36	286	689
m-CNO⁻	2.5×10^{-4}	5	7	24	51
p-CNO⁻	5.3×10^{-4}	7	9	24	37

[a] pH=13, [b] pD = 13, [c] 1M KOH

deactivation processes of the cyanophenolate anion in water are associated with the hydrogen-bonding interactions between the phenolate oxygen atom (and/or the cyano group [33]) and water molecules in addition to the electron ejection. A similar remarkable water-induced quenching process for aniline and its derivatives have been reported [29,34].

The extremely weak fluorescence of the anions of PhOH and CNOHs makes it difficult to observe their ESPT process by steady-state fluorescence measurements (see Figure IV-3 and Table IV-1). Therefore, time-resolved fluorescence and PA measurements were carried out.

IV-4 *Proton dissociation rate of o-cyanophenol in the S_1 state*

Photoprotolytic reactions of phenols in aqueous solution can be described by a two-step model as shown in Figure IV-2. In the first step, a rapid charge separation takes place and a solvent-stabilized ion pair is formed. This is followed by a diffusion step in which the hydrated proton is removed from the parent molecule. Agmon and collaborators [10] have shown that this latter step is described by the Debye-Smoluchowski equation (DSE). In Figure IV-2 k_{dis} and k_{rec} denote the rate constants for adiabatic proton dissociation and reprotonation reactions. Since the decay rate of RO$^-$* is very fast (see Table IV-1), the geminate-recombination (k_{rec}) can be neglected as described in Appendix C. The diffusion second step in Figure IV-2 can also be neglected under moderately acidic conditions ([H$_3$O$^+$] < 10^{-2}M) [35]. Then the fluorescence kinetics of ^{1}ROH* and ^{1}RO$^-$* on excitation by a δ-pulse follows the monoexponential and biexponential laws, respectively:

$$I_f^{ROH}(t) = A_0 \exp\left(-\frac{t}{\tau}\right) \tag{IV-1}$$

$$I_f^{RO^-}(t) = A_0' \left[\exp\left(-\frac{t}{\tau'}\right) - \exp\left(-\frac{t}{\tau}\right) \right] \tag{IV-2}$$

where $1/\tau = k_f + k_{nr} + k_{dis} = 1/\tau_0 + k_{dis}$.

In order to determine the proton dissociation rate from $^1ROH^*$, the fluorescence time profile of o-CNOH in H_2O (pH 2.9) was taken by using the third harmonic (266nm) of the mode-locked Ti:sapphire laser as the excitation source. In Figure IV-5, the fluorescence time profiles of the shorter-wavelength band (monitored at 310nm) and the longer-wavelength band (monitored at 420nm) of o-CNOH are shown along with the least-squares fitting curves based on equations IV-1 and IV-2. The solid lines represent the deconvoluted best fit of (a) a single exponential function and (b) a two-exponential function superimposed on the experimental data points, by using the parameters $\tau = 15$ ps and $\tau' = 31$ ps. It can be seen that both time profiles are well fitted by the kinetics described above; that is, the shorter-wavelength fluorescence band originates from the protonated form (o-CNOH) and the longer-wavelength fluorescence band is due to the deprotonated form (o-CNO$^-$) produced by proton dissociation in the excited state. The decay time constant (31 ps) of the long-wavelength band is actually consistent with the lifetime (30 ps) of o-CNO$^-$ (see Table IV-1). The proton-dissociation rate constant (k_{dis}) of o-CNOH in H_2O was determined to be 6.6 x 10^{10}s^{-1} from the proton dissociation time ($\tau = 15$ps) by using the following equation:

$$k_{dis} = 1/\tau - 1/\tau_0 \tag{IV-3}$$

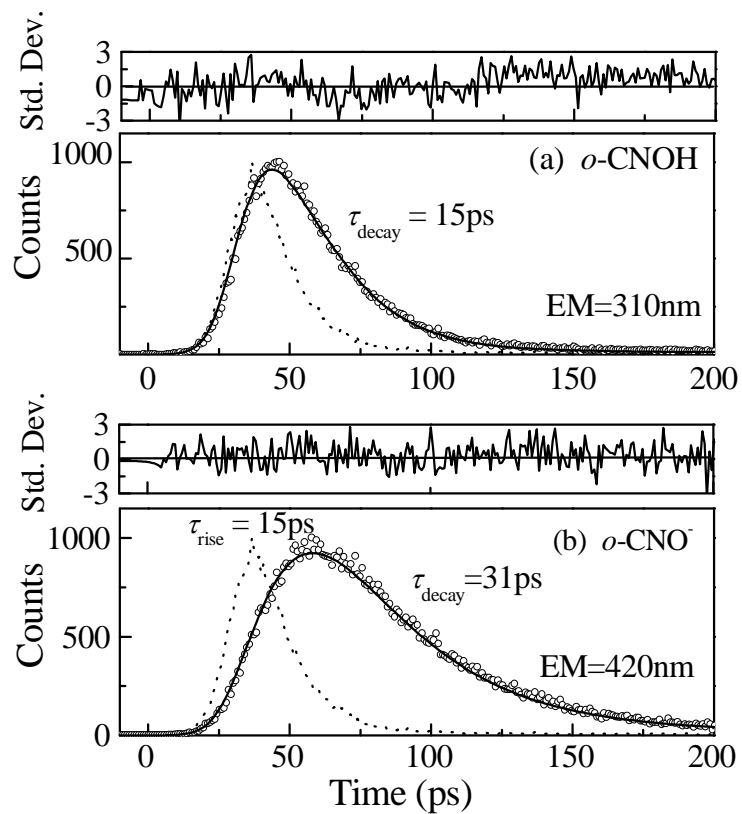**Figure IV-5.** Fluorescence time profiles of *o*-CNOH in H_2O (pH 2.9) at 298K monitored at (a) 310 nm and (b) 420 nm (λ_{exc}=266nm). The instrument response function is denoted by broken line. Standard deviation in (a) is worse than in (b) because of very weak fluorescence intensity at 310nm.

where τ_0 was assumed to be equal to the lifetime (2.0ns) of o-CNOCH$_3$ in H$_2$O (see Table IV-2). It is noted that the proton dissociation rate of o-CNOH in H$_2$O is faster than those of 1-naphthol (2.5 x 10^{10}s^{-1}) and 2-naphthol (1.1 x 10^{8}s^{-1}) [12,13].

IV-5   *Fluorescence lifetimes of phenol and cyanophenols and their methoxy analogues*

Although it has become apparent from the steady-state and time-resolved fluorescence measurements that o-CNOH in H$_2$O undergoes rapid proton transfer to solvent water in the S$_1$ state, it is still not clear whether the proton dissociation takes place similarly in the other compounds (PhOH, m-CNOH, and p-CNOH). If the proton dissociation process, which can compete with the other relaxation processes from the excited state (fluorescence, intersystem crossing, internal conversion, etc.) is involved also in these compounds, the fluorescence lifetimes should become much shorter than those of their methoxy analogues in which the proton cannot be split off. Hence, the fluorescence lifetime of PhOH and CNOHs and their methoxy analogues in H$_2$O and in organic solvents, cyclohexane (CH) and acetonitrile was measured. The fluorescence time profiles of these compounds followed single exponential decay and the fluorescence lifetimes were obtained as shown in Table IV-2. For the compounds with moderate acidity, it can be expected that the ESPT does not occur in organic solvents [9]. Actually, the fluorescence lifetimes of PhOH and CNOHs in organic solvents are relatively long (2.0-7.0ns), and are only slightly shorter than those of their methoxy analogues both in CH and CH$_3$CN. In contrast to the lifetimes in organic solvents, the fluorescence lifetimes of CNOHs in H$_2$O are remarkably short. In particular, the lifetime (0.015ns) of o-CNOH is extremely short, which was ascribable to fast proton dissociation in the excited state. In the same manner, the

short lifetime (0.037ns) of *m*-CNOH in H_2O suggests the occurrence of the excited-state proton dissociation. The lifetime of *p*-CNOH in H_2O is one-order of magnitude longer than those of *o*- and *m*-CNOH in H_2O. Although the lifetime of *p*-CNOH in H_2O is much shorter than those in CH and CH_3CN, the methoxy analogue (*p*-CNOCH$_3$) also shows a similar tendency. It is therefore not clear whether proton dissociation occurs in *p*-CNOH or not.

IV-6   *Volume changes associated with ESPT of PhOH and CNOHs in water*

In order to examine the ESPT of PhOH and CNOHs in more detail, photoacoustic (PA) measurements were carried out [36]. The amplitude of PA signal H is attributable to the overall volume change arising from two contributions,

$$H = k\left(\Delta V_{\text{th}} + \Delta V_{\text{r}}\right) \qquad\qquad \text{(IV-4)}$$

where k is the instrumental constant, ΔV_{th} is the volume change of the solvent due to heat released by nonradiative deactivation process, and ΔV_{r} (ml Einstein^{-1}) is the structural volume change per absorbed Einstein, which includes any conformational variation due to photochemical processes and/or rearrangement of solvent. ΔV_{th} is related to the thermodynamic parameters as follows,

$$\Delta V_{\text{th}} = \alpha\left(\frac{\beta}{C_p\rho}\right)E_\lambda \qquad\qquad \text{(IV-5)}$$

where α is the fraction of absorbed energy released as heat within the effective

Table IV-2: Fluorescence Lifetimes of Phenol, Cyanophenols and Their Methoxy Analogues in H_2O, CH and CH_3CN at 298K[a]

compound	τ_f (ns)		
	H_2O	CH	CH_3CN
PhOH	3.1	2.4	6.4
o-CNOH	0.015[b]	3.6	2.1
m-CNOH	0.037	4.3	2.7
p-CNOH	0.32	5.7	2.7
PhOCH$_3$	5.0	8.6	7.7
o-CNOCH$_3$	2.0	3.9	2.8
m-CNOCH$_3$	1.4	4.6	3.7
p-CNOCH$_3$	0.87	5.5	6.4

[a] monitored at fluorescence peak wavelengths

[b] monitored at 310nm

acoustic transit time, β is the thermal expansion coefficient of the solvent, C_p is the specific heat capacity of the solvent, ρ is mass density of the solvent, and E_λ is the excitation energy per absorbed Einstein (450 kJmol^{-1} at 266 nm). The structural volume change per photoconverted mole ΔV_R (ml mol^{-1}) is derived by using the reaction quantum yield Φ_R producing RO$^-$ and H$_3$O$^+$ (see Figure IV-2):

$$\Delta V_R = \Delta V_r / \Phi_R \qquad\qquad \text{(IV-6)}$$

Sodium dichromate (Na$_2$Cr$_2$O$_7$) was used as a photocalorimetric reference in aqueous solution at 266nm excitation. The thermal conversion efficiency α of Na$_2$Cr$_2$O$_7$ can be assumed to be unity [36e]. The PA signal amplitude of the photocalorimetric reference at temperature T is represented by

$$H_T^R = k\Delta V_{\text{th}} = k\left(\frac{\beta}{C_p\rho}\right)E_\lambda \qquad\qquad \text{(IV-7)}$$

At the temperature $T_{\beta=0} = 3.9°C$ for which the thermal expansion coefficient of water is zero, the PA signal of the sample solution $H_{T_{\beta=0}}^S$ is given by the structural volume change alone:

$$H_{T_{\beta=0}}^S = k\Delta V_r \qquad\qquad \text{(IV-8)}$$

Therefore, ΔV_r can be related to the ratio of $H_{T_{\beta=0}}^S$ to H_T^R as

$$\frac{H_{T_{\beta=0}}^S}{H_T^R} = \frac{\Delta V_r}{E_\lambda}\left(\frac{C_p\rho}{\beta}\right) \qquad\qquad \text{(IV-9)}$$

The measurement of the structural volume change based on equation IV-9 is called two-temperature method [36]. Thus, ΔV_r can be estimated by taking the PA signal ratio of the sample at $T_{\beta=0}$ to the reference at T.

If an excited cyanophenol molecule dissociates into a solvent-stabilized ion pair in water, substantial volume contraction arising from electrostriction of water around the ions is expected to occur. Figure IV-6 shows the PA signals of PhOH and CNOHs in H_2O at 3.9 °C, along with the signal of $Na_2Cr_2O_7$. They were obtained for the solutions with almost the same absorbance (~0.2) at the excitation wavelength. The reference compound $Na_2Cr_2O_7$ is known to deactivate very rapidly from the excited state with a quantum yield of nearly unity; that is, it releases all the excitation photon energy as heat. The almost no signal of $Na_2Cr_2O_7$ in Figure IV-6 clearly shows that the contribution of thermal expansion to PA signal is negligible under this condition and the PA signal originates solely from structural volume changes. For *o*- and *m*-CNOH, clear PA signals, which correspond to volume contractions, are seen. On the basis of the deconvolution analyses of the PA waveforms, the volume changes per absorbed Einstein (ΔV_r) for *o*- and *m*-CNOH were obtained to be -5.0 and -2.4 mL Einstein^{-1}, respectively (see Appendix B.). The volume contraction per mole (ΔV_R) can be calculated from equation IV-6 by using the formation quantum yield $\Phi(RO^-)$ of free RO^-. As can be seen from Figure IV-2, $\Phi(RO^-)$ would be less than unity even if the quantum yield of proton dissociation ($\Phi_{dis} = k_{dis}/(k_f + k_{nr} + k_{dis})$) is unity, because the rapid decay of ($RO^{-*} \cdots H_3O^+$) is expected to lead to the geminate recombination in the ground-state ion pair. The geminate recombination yield is denoted by $1-\eta$ in Figure IV-2.

The volume contraction following proton dissociation of excited 1-naphthol in

water was measured by means of the PA method, and ΔV_R = -16.4 mL mol^{-1} was obtained (see Appendix B.). This is in good agreement with the value (ΔV_R = -15.8 mL mol^{-1}) [37] obtained by similar PA measurements and that (ΔV_R = -17.2 mL mol^{-1}) [38] measured by dilatometry. By assuming that the quantum yield for the formation of free RO$^-$ (Φ(RO$^-$)) from o-CNOH is unity, the volume contraction (ΔV_R) accompanying the ESPT reaction of o-CNOH becomes -5.0 mL mol^{-1}, which is much smaller than the ΔV_R values (-12.9 and -13.0 mL mol^{-1}, respectively) [39] estimated from the partial molar volumes for the ground-state proton dissociation reactions of m-CNOH and p-CNOH (the partial molar volumes related to ΔV_R of o-CNOH were not available in the literature). An explanation for this disagreement can be proposed as follows. As shown in Figure IV-2, if the geminate recombination in the ground-state ion pair (RO$^-\cdots$H$_3$O$^+$) occurs after rapid deactivation of the excited ion pair (RO$^-*\cdots$H$_3$O$^+$), Φ(RO$^-$) becomes less than unity, and the apparent volume contraction might become significantly smaller than the value calculated by partial molar volumes. As is pointed out by Agmon [35], if the acidity of a ground-state molecule is much smaller than that in the S$_1$ state, as in the case of naphthols and phenols, a considerable fraction of the ion pairs produced by an ESPT reaction may recombine in the ground state. Because the recombination probability is larger for pairs which have not separated too much while in the excited state, the ground-state recombination probability is expected to be larger for an excited molecule with a
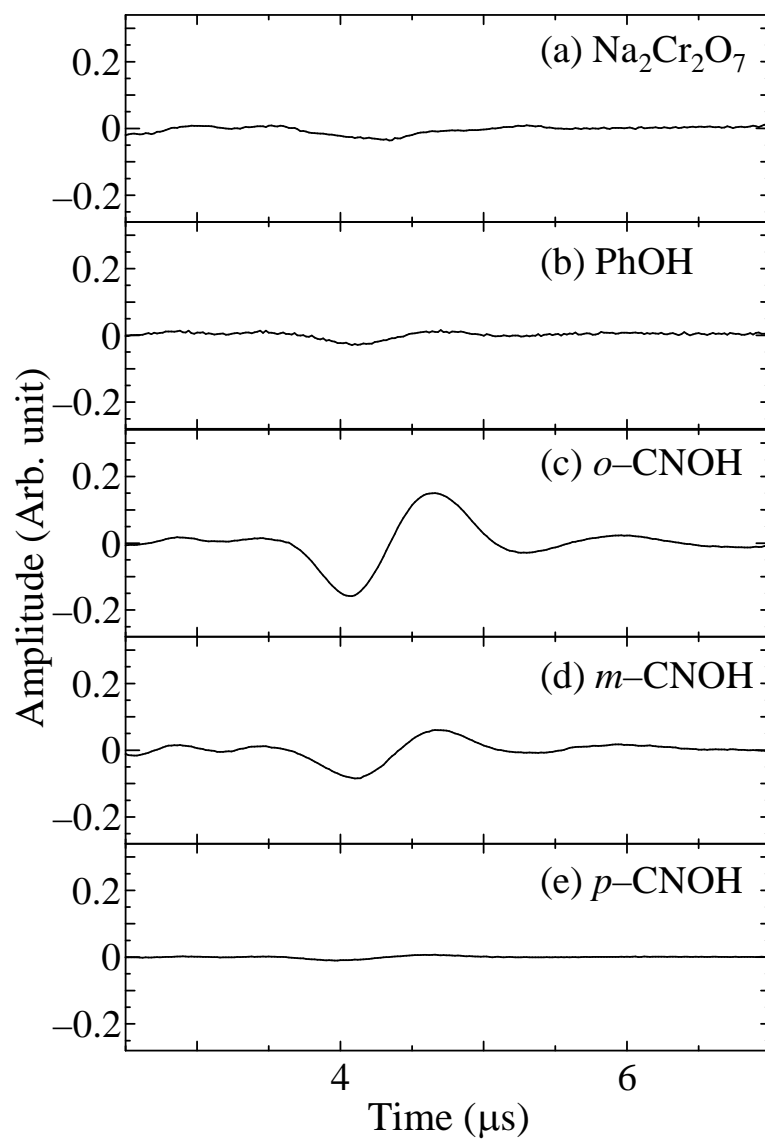
Figure IV-6. PA signals for (a) the calorimetric reference $Na_2Cr_2O_7$, (b) PhOH, (c) o-CNOH, (d) m-CNOH, and (e) p-CNOH in H_2O (pH 4.0) at 3.9 °C.

shorter S_1 lifetime. The extremely short lifetimes of o-CNO^{-*} and m-CNO^{-*} are consistent with the explanation of the observed volume contraction on the basis of ground-state geminate recombination. If one assumes that for o-CNOH the quantum yield of proton dissociation (Φ_{dis}) is unity and the magnitude of ΔV_R is the same as those (13 mL mol^{-1}) of m-CNOH and p-CNOH, the η value in Figure IV-2 can be estimated to be 0.38.

The volume contractions observed for o- and m-CNOH demonstrate the occurrence of ESPT process which results in ion-pair formation. From the fluorescence decay time (37 ps) of m-CNOH and that (1.4 ns) of m-CNOCH$_3$ in H$_2$O, the proton dissociation rate constant of m-CNOH was estimated to be 2.6 x 10^{10}s^{-1}, which is somewhat smaller than that of o-CNOH.

IV-7 *Proton dissociation of cyanophenols in the excited state*

The proton-dissociation rate constant of o- and m-CNOH in H$_2$O and D$_2$O was measured under different temperatures. The Arrhenius plot of the obtained k_{dis} values is depicted in Figure IV-7. In the temperature range between 275 and 323 K, a linear relationship between lnk_{dis} and $1/T$ is seen for both the H$_2$O and D$_2$O solutions, respectively. From the straight lines in Figure IV-7, the activation energies for the proton dissociation reactions of o-CNOH in H$_2$O and D$_2$O were obtained to be 7.3 and 8.8 kJmol^{-1}, respectively (see Table IV-3). For m-CNOH, somewhat larger E_a values, 10 and 13 kJmol^{-1}, were found for the H$_2$O and D$_2$O solutions. In both compounds, the D$_2$O solution gives a slightly larger E_a value compared to that of the H$_2$O solution (see Table IV-3). In order to compare the proton dissociation rate with the solvent relaxation rate, the inverse of the Debye dielectric relaxation time (τ_D) of H$_2$O and D$_2$O [40-42] is plotted as a function of $1/T$ in Figure IV-7. It can be seen that the proton dissociation rate of o- and m-CNOH in H$_2$O and D$_2$O is slower than the solvent relaxation rate evaluated from the Debye dielectric relaxation time,

which is related to the collective structural rearrangement of the hydrogen-bonded liquid enabling the individual molecules to reorient [42]. In addition, much larger deuterium isotope effects are seen in the proton transfer rates of *o*- and *m*-CNOH as compared with those in the solvent relaxation rate. This behavior is in accord with an activation-controlled reaction along the proton coordinate.

Robinson et al. [12,14] and Huppert et al. [43] have reported that weak photoacids, such as 2-naphthol, behave in an Arrhenius fashion, giving a linear dependence of lnk_{dis} on $1/T$ between the freezing and boiling temperatures of water. Its activation energy is $E_a \approx 11$ kJmol^{-1}. Only in supercritical or supercooled water, some downward deviation from the Arrhenius behavior is seen. In contrast, stronger photoacids, such as 8-hydroxypyrene-1,3,6-trisulfonate [15] or 2-hydroxynaphthalene-6,8-disulfonate in water, exhibit a strongly curved Arrhenius plot; that is, the reaction activation energy is temperature-dependent. These compounds and also 1-naphthol[12] have $E_a \approx 0$ at high temperatures, suggesting a negligible barrier along the proton coordinate. Huppert et al. [15] have suggested that at low temperatures, solvent motion with characteristic time close to τ_D controls the proton transfer rate, whereas at the high-temperature limit, the solvent-relaxation time is faster than the passage of the proton over the barrier, and the overall rate constant is determined by the proton motion. The kinetic behavior of *o*-CNOH in H$_2$O and D$_2$O seems to be somewhat different from that of the above compounds. The prototropic properties of *o*-CNOH, as exemplified by the pK_a* value (-0.5) and
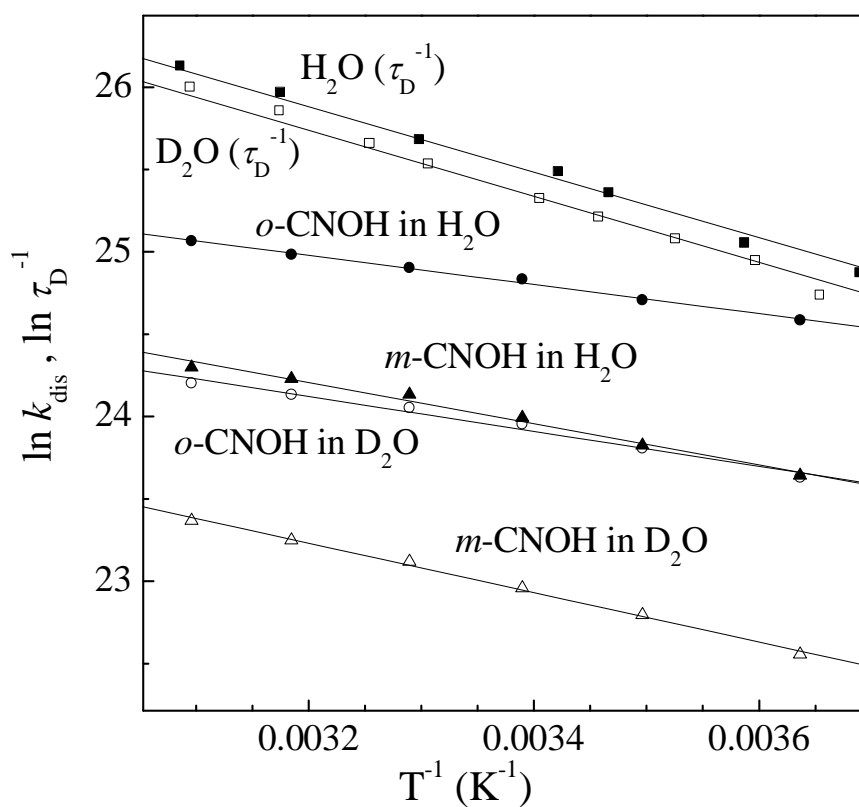
Figure IV-7. Arrhenius plot of the proton-dissociation rate constant of *o*-CNOH in H$_2$O (pH 2.9) and D$_2$O (pD 2.7), *m*-CNOH in H$_2$O and D$_2$O, and the reciprocal of the Debye dielectric relaxation time τ_D in H$_2$O and D$_2$O.

Table IV-3: Proton Dissociation Rate Constant (k_{dis})[a], Activation Energy (E_a), Frequency Factor (A) and Isotope Effect (k_{dis}^H/k_{dis}^D)[a] for ESPT Reactions of Cyanophenols in H_2O (pH 2.9) and D_2O (pD 2.7)

compound	solvent	k_{dis} $(10^{10}s^{-1})$	E_a $(kJmol^{-1})$	A $(10^{12}s^{-1})$	$\dfrac{k_{dis}^H}{k_{dis}^D}$
o-CNOH	H_2O	6.6	7.3	1.2	2.4
	D_2O	2.8	8.8	0.9	
m-CNOH	H_2O	2.6	10	1.6	2.8
	D_2O	0.93	13	1.6	

[a] at 298K

the fast proton-dissociation rate, are in conformity with a relatively strong photoacid. Nevertheless, it has a nearly constant activation energy (7.3 kJmol^{-1} in H_2O) even at higher temperatures.

These results showed that PhOH has moderate acidity ($pK_a^* > 0$), even in the S_1 state, and the the k_{dis} value of PhOH in water can be evaluated to be less than 1.3 x 10^8 s^{-1} from equation IV-3 and Table IV-2. This is in contrast with 1- and 2-naphthols which undergo ESPT in water. The proton dissociation rate in the excited state is enhanced considerably by introducing an electron-withdrawing group at proper position(s). As for PhOH, it was found that the ortho-position is the most effective cite to enhance the excited-state acidity, and the k_{dis} value (6.6 x 10^{10}s^{-1}) was increased more than one-order of magnitude by introducing a cyano group at the *o*-position. The para-position is, on the other hand, found to be less effective to enhance the excited-state acidity; the k_{dis} value is estimated to be less than 2.0 x 10^9s^{-1}. Recently, Hynes et al. [44] have made theoretical investigations on excited-state acidities of PhOH and CNOHs. They have proposed that the n-π* CT on the anion side of the reaction, and not the one of the acid side, is the fundamental origin of the enhanced excited-state acidity. They have also proposed a theoretical equation to calculate the rate constant of proton transfer in hydrogen-bonded acid-base complexes such as phenol-trimethylamine in methyl chloride solvent [45]. The extension of π-electronic systems can also modify the excited-state acidity of PhOH. Recently, Lewis et al. [46] have reported that the 4-cyanohydroxystilbenes undergo ESPT with rate constants of 5 x 10^{11} s^{-1}. These rate constants are comparable to the fastest among the ESPT rate reported so far [34,47,48], and approach the theoretical limit for water-mediated proton transfer.

In recent studies, the neutral form of the chromophore

(*p*-hydroxybenzylidene-imidazolidinone) in wtGFP is reported to undergo ESPT upon photoexcitation and to result in characteristic green (508nm) emission [23-26]. The photophysics of *p*-hydroxybenzylidene dimethylimidazolinone (*p*-HBDI), a model chromophore of GFP, in solution has also been investigated through ultrafast fluorescence spectroscopy [49,50]. The ESPT to solvent in the model compound *p*-HBDI has not been observed because of ultrafast internal conversion through specific structural displacement. The protein-chromophore interaction in wtGFP leads to the suppression of the radiationless decay and should also be responsible for the occurrence of ESPT in GFP. Despite the fact that the chromophore of wtGFP can be regarded as a *p*-substituted phenol, wtGFP is reported to undergo ESPT. This seems to be in conflict with our observation that *p*-substitution is not effective to enhance photoacidity of phenol by introducing an electron-withdrawing CN group. However, the results of Lewis et al. [46] on the 4-cyanohydroxystilbenes seem to suggest that the extension of π-electronic conjugation through the *p*-position can also enhance the photoacidity of phenol.

IV-8 *Conclusion*

The picosecond time-resolved fluorescence measurements of PhOH and CNOHs revealed that *o*- and *m*-CNOH in H_2O undergo ESPT with rate constants of 6.6 x 10^{10} and 2.6 x $10^{10}\,s^{-1}$, respectively, at 298K. These rates are slower than the solvent relaxation rate evaluated from the Debye dielectric relaxation time (τ_D) of water at 298K, which suggests that the overall rate constant is determined by the proton motion along the reaction coordinate. The photoacoustic spectroscopy was used as a complementary method to examine the ESPT of PhOH and CNOHs. The analysis of the obtained photoacoustic signals showed that photoexcitation of *o*-CNOH and *m*-CNOH in H_2O results in volume changes (ΔV_r) of -5.0 and -2.4 mL Einstein^{-1}, respectively. The observation of volume contractions is consistent with the occurrence of ESPT which gives a solvent-separated ion pair (hydrated proton and phenolate anion). In contrast to *o*- and *m*-CNOH, the excitation of PhOH and *p*-CNOH in H_2O showed negligibly small volume changes. The results of photoacoustic measurements and the fluorescence properties of PhOH and *p*-CNOH indicate that the ESPT rates of these compounds are significantly slower than those of *o*- and *m*-CNOH, and the occurrence of ESPT could not be verified clearly from their fluorescence properties in water. The introduction of a strongly electron-withdrawing group at *o*- or *m*-position in PhOH substantially enhances the proton transfer ability to solvent in the excited state. If one assume that the quantum yields of the solvent-separated ion pair are unity, the volume changes per mole (ΔV_R) of *o*-CNOH and *m*-CNOH in H_2O were estimated to be -5.0 and -2.4 mL mol^{-1}, respectively, which were much smaller than the ΔV_R values (-12.9 mL mol^{-1} and -13.0 mL mol^{-1}, respectively [39]) estimated from partial molar volumes for the ground-state proton dissociation reactions for *m*-CNOH and *p*-CNOH. The

disagreement could be attributed to the involvement of ground-state geminate recombination between the ejected proton and cyanophenolate anion after rapid deactivation of the excited ion pair.

Appendix B.

Deconvolution analyses of PA waveform

The PA signal $S(t)$ of sample solutions is expressed as convolution integral between impulse response function $R(t)$ and time-dependent sample decay function $h(t)$.
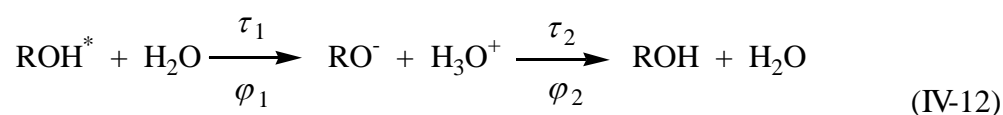
$$S(t) = R(t) \otimes h(t) \tag{IV-10}$$

where $R(t)$ is given by the PA signal of photocalorimetric reference. In a sequential reaction model, $h(t)$ is given by

$$h(t) = \sum_i \varphi_i h_i(t) = \frac{\varphi_1}{\tau_1} \exp\left(-\frac{t}{\tau_1}\right) + \frac{\varphi_2}{\tau_1 - \tau_2}\left[\exp\left(-\frac{t}{\tau_1}\right) - \exp\left(-\frac{t}{\tau_2}\right)\right] \tag{IV-11}$$

where $h_i(t)$ is the sample decay function of the transient i with the lifetime of τ_i and φ_i is the fractional amplitude.

The ESPT cycle of hydroxyaromatic molecules can be analyzed according to a sequential reaction scheme:

$$\text{ROH}^* + \text{H}_2\text{O} \xrightarrow[\varphi_1]{\tau_1} \text{RO}^- + \text{H}_3\text{O}^+ \xrightarrow[\varphi_2]{\tau_2} \text{ROH} + \text{H}_2\text{O} \tag{IV-12}$$

where φ_1 is the PA signal amplitude for the proton transfer step with the time constant of τ_1, φ_2 is that for the proton recombination process with the time constant of τ_2. The parameters φ_1, τ_1, φ_2, τ_2 can be calculated from the sample and reference PA waveforms by means of the deconvolution method. The deconvolution analyses of the waveform were performed using the Sound Analysis 3000 software (Quantum Northwest). Figure S1(a) shows the PA signal of photocalorimetric reference $\text{Na}_2\text{Cr}_2\text{O}_7$ in H_2O (pH 4.0) at

10°C, which corresponds to the impulse response function $R(t)$, and the PA signal $S(t)$ of o-CNOH in H_2O (pH 4.0) at 3.9°C ($T_{\beta=0}$). Figure S1(b) shows the deconvoluted sample signals:

$$S(t) = S_1(t) + S_2(t) \qquad\qquad\text{(IV-13)}$$

where $S_1(t)$ is the negative volume change signal ($\varphi_1 = -0.476$ and $\tau_1 < 1ns$) due to the photo-induced proton transfer reaction, and $S_2(t)$ is the positive volume change signal ($\varphi_2 = 0.471$ and $\tau_2 = 217ns$) arising from the proton recombination reaction.

By applying the deconvolution analysis to equation IV-6 in the text, the following equation is derived:

$$\varphi_1 E_\lambda = \Delta V_r \left(\frac{C_p \rho}{\beta} \right) \qquad\qquad\text{(IV-14)}$$

In the two-temperature method using deconvolution analyses, the structural volume change per absorbed Einstein (ΔV_r) can be determined from the plot of $\varphi_1 E_\lambda$ versus the thermodynamic parameters term ($C_p \rho / \beta$). In Figure IV-9 the values of φ_1 obtained for the proton dissociation step of o-CNOH and 1-naphthol (1-NpOH) in H_2O (pH 4.0) are plotted following equation IV-14. From the slopes of the straight lines, ΔV_r were obtained as -5.0 and -11.1 mL Einstein^{-1} for o-CNOH and 1-naphthol, respectively. By using the reaction quantum yield ($\Phi_R = 0.68$) for 1-NpOH, which was estimated by transient absorption measurements, the structural volume change per photoconverted mole ΔV_R of 1-NpOH was obtained to be -16.4 mL mol^{-1}.
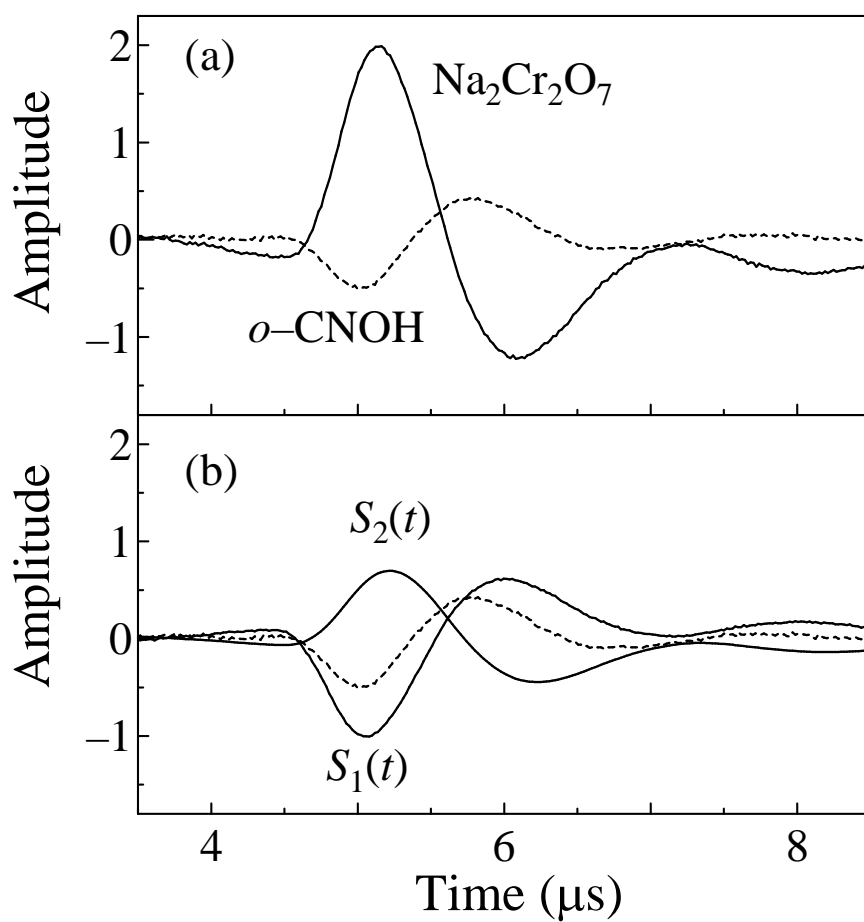
Figure IV-8. (a) PA signal amplitudes of photocalorimetric reference $Na_2Cr_2O_7$ in H_2O (pH 4.0) at 10°C (solid line) and o-CNOH in H_2O (pH 4.0) at 3.9°C (broken line), and (b) the deconvoluted sample signals $S_1(t)$ and $S_2(t)$. PA signal amplitude of o-CNOH in H_2O is shown both in (a) and (b) as broken line.
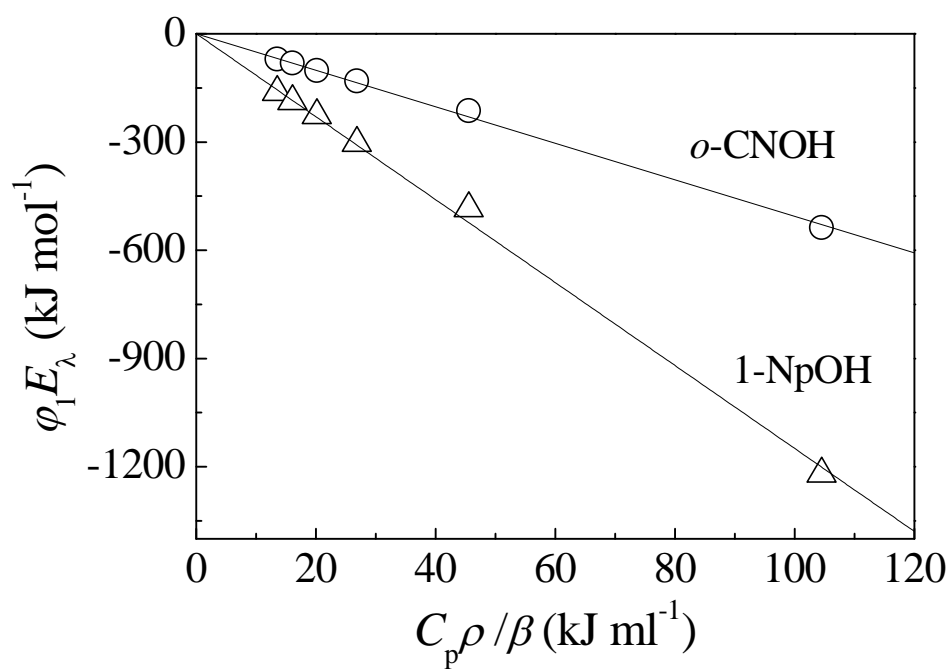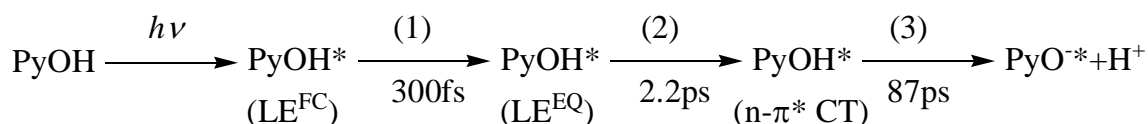
Figure IV-9. $\varphi_1 E_\lambda$ value vs ($C_p\rho/\beta$) for the PA signals obtained by excitation of o-CNOH (open circle) and 1-NpOH (open triangle) in H_2O (pH 4.0).

Appendix C.

long-time asymptotic behavior of photoacid hydroxyarene

Hynes et al. have proposed a new perspective (a three step mechanism) on intermolecular photochemical proton transfer in solution [44,51,52]. They performed femtosecond fluorescence and absorption measurements on pyranine (8-hydroxy-1,3,6- trisulfonate pyrene) in aqueous solution, and found that the early events of photo-induced proton transfer from pyranine to water involve three successive steps: two ultrafast steps (300fs and 2.2ps) which precede the relatively slow (87ps) proton transfer step. Scheme IV-1 shows summary of their femtosecond experiments on pyranine in aqueous solution [44,51,52].
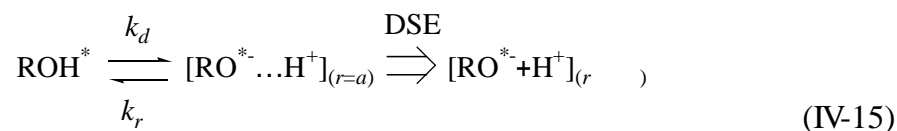
$$\text{PyOH} \xrightarrow{h\nu} \underset{(LE^{FC})}{\text{PyOH*}} \xrightarrow[300fs]{(1)} \underset{(LE^{EQ})}{\text{PyOH*}} \xrightarrow[2.2ps]{(2)} \underset{(n\text{-}\pi^* \ CT)}{\text{PyOH*}} \xrightarrow[87ps]{(3)} \text{PyO}^{-}\text{*}+\text{H}^{+}$$

Scheme IV-1

The first step (less than 300fs) is attributable to solvation dynamics of the Franck-Condon S_1 state (LE^{FC}) of pyranine produced by femtosecond laser pulse excitation to produce the equilibrium S_1 state (LE^{EQ}). The second step, with a time constant of 2.2ps, accompanies some change in oscillator strength, which is not found for the first or last step. This suggests that the second step is associated with a change in electronic state, i.e., from locally excited state (or ^1L_b state) to n-π* charge transfer state (or ^1L_a state). The latter state involves partial charge migration from the oxygen of the OH into the ring system, but no PT is involved in this step. The third step involve n-σ* charge transfer, i.e., CT from the nonbonding orbital of the base to

the antibonding orbital of the acid, and this step corresponds to the PT step itself [44]. Participation of n-σ* CT in PT reactions has been originally proposed for the ground state reactions [53]. The PT picture depicted in Scheme IV-1 demonstrates that the electronic rearrangements associated with the proton transfer act is a crucial aspect of PT reactions in solution.

Ultrafast measurements of fluorescence decay curves of photoacids have revealed the important contribution of geminate recombination (neutralization) of the two separated ions in the overall geminate process, by nonexponential decay profiles [15,35a,35c,53-59]. Pines and Huppert [54] have reported the first direct detection of geminate recombination kinetics in ESPT. The fluorescence decay profile of hydroxyarene (ROH) obtained by picosecond laser pulse excitation showed non-exponential behavior with a long-time tail. This has been attributed to a reversible time-dependent geminate recombination. The reprotonation is an adiabatic process, so that the excited ROH* can undergo a second cycle of deprotonation. Based on the experimental and theoretical studies, Agmon, Pines, and Huppert [35a,56,57] have analyzed the overall kinetics according to a two-step mode:

$$\text{ROH}^* \underset{k_r}{\overset{k_d}{\rightleftharpoons}} [\text{RO}^{*-}...\text{H}^+]_{(r=a)} \overset{\text{DSE}}{\Longrightarrow} [\text{RO}^{*-}+\text{H}^+]_{(r\quad)} \tag{IV-15}$$

The first step, which is described by back-reaction boundary condition with intrinsic rate constate k_d and k_r, is followed by a diffusional second step in which the hydrated proton is removed from the parent molecule. Separation of a contact ion pair from the contact radius, a, to infinity is described by the transient numerical solution of the Debye-Smoluchowski equation (DSE). The asymptotic expression

(the long time behavior) for the fluorescence of ROH*(t) is derived as [59]

$$[\text{ROH}^*] \cong \frac{\pi}{2} a^2 \exp(R_D/a) \frac{k_r}{k_d (\pi D)^{3/2}} t^{-3/2} \tag{IV-16}$$

In equation IV-16, $D = D_{\text{H}^+} + D_{\text{RO}*^-}$ is the mutual diffusion coefficient of the proton and its conjugate base, and R_D is Debye radius, given by

$$R_D = \frac{|z_1||z_2|e^2}{\varepsilon k_B T} \tag{IV-17}$$

where z_1 and z_2 are the charges of the proton and anion, and e is the static dielectric constant of the solvent. Equation IV-16 predicts that the time-dependent population of ROH* conforms to power law at $t^{-3/2}$. However, Agmon et al. proposed the diffusion kinetics model, which is controlled by the difference in lifetime of neutral and anion speices [35b]. They claim that when deprotonated species decays faster than protonated species, there is no time for diffusional effects to accumulate, and both decay become exponential.

However, despite a large number of experimental studies for many naphthol derivatives, there is little experimental evidence to directly confirm the validity of this model that switches from power law to exponential decay [10]. To verify the theoretical prediction, they have examined naphthol derivatives with particularly short anion lifetimes, and found 5-(methanesulfonyl)-1-naphthol as the appropriate molecule in organic solvents [35c]. However, this molecule cannot be used in water.

Thus, conjugated anions of phenol analogue in water have remarkably short fluorescence lifetimes, so that study of ESPT for phenol analogues is important to consider the validity of the theoretical prediction. Therefore, asymptotic

fluorescence behavior of phenol analogues allows testing directly some of the theoretical predictions for DSE model in AB regime.

Excited-state proton transfer reaction to solvent from excited hydroxyarene is schematically depicted by

$$AB \quad \underset{W_a(r)}{\overset{W_d(r)}{\rightleftarrows}} \quad A+B$$

$$\downarrow k_0 \qquad\qquad \downarrow k_0'$$

(IV-18)
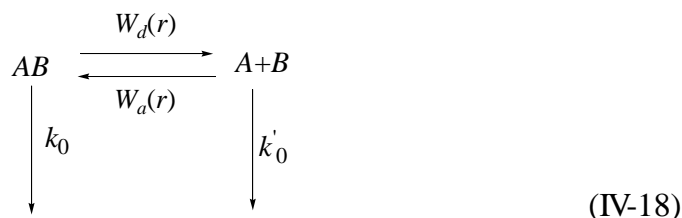
where k_0 and k_0' are the reciprocal excited state lifetimes of the neutral species (*AB*) and anion species (*B*), respectively. Debye-Smoluchowski equation (DSE) in three dimensions, which is coupled to a kinetic equation for $p(t)$,

$$\frac{\partial}{\partial t} p(r,t) = Lp(r,t) - [W_a(r) + k_0']p(r,t) + W_d(r)p(*,t) \qquad \text{(IV-19)}$$

$$\frac{\partial}{\partial t} p(*,t) = 4\pi \int_a^\infty W_a(r) \, p(r,t) r^2 \mathrm{d}r - (k_d + k_0) p(*,t) \qquad \text{(IV-20)}$$

Here *L* is the spherically symmetric Smoluchowski operator in three dimensions, given by

$$L \equiv r^{-2} \frac{\partial}{\partial r} D(r) r^2 e^{-V(r)} \frac{\partial}{\partial r} e^{V(r)} \qquad \text{(IV-21)}$$

The approximate solution to equations IV-19 and IV-20 can be subsequently written in terms of two roots of a quadratic polynomial that appears in the denominator of the approximate Laplace transform,

$$\sigma_{\pm} = \frac{k_{off} a'_{eff}}{2D}(-1 \pm \sqrt{(1+\beta)}) \qquad \text{(IV-22)}$$

The ultimate "escape probability", Z, is given by

$$Z = \frac{k_{off}}{k_{off} + k'_0 - k_0} \qquad \text{(IV-23)}$$

Here β is the dimensionless parameter

$$\beta \equiv \frac{4D(k_0' - k_0 - k_{off})}{(k_{off} k'_{eff})^2} \qquad \text{(IV-24)}$$

These roots enter into the special function

$$\phi_{\pm} = \exp(\sigma_{\pm}^2 Dt)\text{erfc}(-\sigma_{\pm}\sqrt{Dt}) \qquad \text{(IV-25)}$$

where erfc(x) is the complementary error function for a possibly complex argument, x. The approximate protonation and separation probabilities are finally written as

$$p(r_0, t \mid r_0) = \frac{e^{-k_D't}}{2}\left(\phi_+(t) + \phi_-(t) - \frac{\phi_+(t) - \phi_-(t)}{\sqrt{1+\beta}}\right) \qquad \text{(IV-26)}$$

$$S(t \mid r_0) = \frac{e^{-k_D't}}{\sqrt{1+\beta}}\left(\frac{(1+\sigma_+ a'_{eff})\phi_+(t) - 1}{\sigma_+ a'_{eff}} - \frac{(1+\sigma_- a'_{eff})\phi_-(t) - 1}{\sigma_- a'_{eff}}\right) \qquad \text{(IV-27)}$$

where $p(r_0, t \mid r_0)$ is the protonation probability which corresponds to the fluorescence lifetime of neutral species (AB), $S(t \mid r_0)$ is the separation probability

which corresponds to the fluorescent lifetime of anion species (A).

It is reported to be classify an asymptotic solution to the long-term behavior of fluorescence lifetime in the neutral and the anion.

$$p(r_0, t \mid r_0) \approx Z^2 \frac{K_{eq}}{(4\pi Dt)^{3/2}} e^{-k_0't} \tag{IV-28}$$

$$S(t \mid r_0) \approx \left[1 + \frac{K_{eq}(k_0 - k'_0)Z}{4\pi D} \frac{1}{\sqrt{\pi Dt}} \right] e^{-k_0't} \tag{IV-29}$$

When fluorescence decay lifetime of the anion is longer than that of the neutral,

$$p(r_0, t \mid r_0) \approx \left(1 - \frac{1}{\sqrt{1+\beta}} \right) e^{[\ (k_0 + k_{off}(1+\sigma_+ a'_{eff}))t]} \tag{IV-30}$$

$$S(t \mid r_0) \approx \frac{2}{\sqrt{1+\beta}} \frac{1 + \sigma_+ a'_{eff}}{\sigma_+ a'_{eff}} e^{[\ (k_0 + k_{off}(1+\sigma_+ a'_{eff}))t]} \tag{IV-31}$$

When A decays faster than AB ($\beta > 0$), there is no time for diffusional effects to accumulate, and the decay become exponential (see Figure IV-5) In this case the system is most of the time in the AB state, so it is termed the "AB regime".

Figure IV-10 show the log-log plot of correlated fluorescence decay curve of o-CNOH and NpOH in aqueous solution at 293 K. Each log-log plot of correlated fluorescence decay curve gives quiet different picture.

Temperature dependences of the fluorescence properties of CNO^- in different solvents are shown in Tables IV-4 and IV-5. It is clear that the phenolate anions depend on the solvent proticity and the temperature. Thus, time-resolved

fluorescence experiment of phenols under controlled condition such as water amount as solvent or the temperature, it may help to confirm the asymptotic fluorescence behavior predicted by DSE model under different situation.

Table IV-4. Temperature effect on the fluorescence lifetime of phenolate (PhO⁻) and cyanophenolate anions (CNO⁻) in H_2O and D_2O.

| | PhO⁻ | | | o-CNO⁻ | | | m-CNO⁻ | | | p-CNO⁻ | | |
| | τ_f /ps | | KIE[a] | τ_f /ps | | KIE | τ_f /ps | | KIE | τ_f /ps | | KIE |
T/K	H_2O	D_2O		H_2O	D_2O		H_2O	D_2O		H_2O	D_2O	
273	46	107	2.3	40	49	1.2	7.4	9.7	1.3	12	15	1.3
286	28	66	2.4	34	41	1.2	5.7	7.9	1.4	9.2	12	1.3
295	18	43	2.4	30	36	1.2	5.4	6.9	1.3	7.2	9.0	1.3
305	13	31	2.4	28	33	1.2	5.0	6.2	1.2	6.3	8.0	1.3
315	10	22	2.2	26	30	1.2	4.6	5.5	1.2	5.9	7.7	1.3
328	7	13	1.9	23	27	1.2	3.8	4.7	1.2	4.4	6.3	1.4
E_a / kJmol⁻¹	27	29		7.8	8.3		8.5	10		13	12	
A/ 10^{12}s⁻¹	2480	3330		0.8	0.8		5.7	8.6		27	13	

[a] KIE = $(\tau_f^H)^{-1}/(\tau_f^D)^{-1}$

Table IV-5. Temperature effect on the fluorescence lifetime of phenolate and cyanophenolate anions (CNO⁻s) in MeOH and EtOH.

	τ_f /ps							
	PhO⁻		o-CNO⁻		m-CNO⁻		p-CNO⁻	
T/K	MeOH	EtOH	MeOH	EtOH	MeOH	EtOH	MeOH	EtOH
275	500	588	441	906	37	80	34	56
285	426	544	349	733	30	65	28	45
298	345	477	286	689	24	51	24	37
305	280	405	251	536	22	42	21	32
314	215	332	218	456	18	35	18	27
328	149	229	180	381	15	28	15	23
Ea / kJmol⁻¹	17	13	13	12	12	15	11	13
A/ 10^{11}s⁻¹	33	4.7	5.6	2.4	63	99	42	53
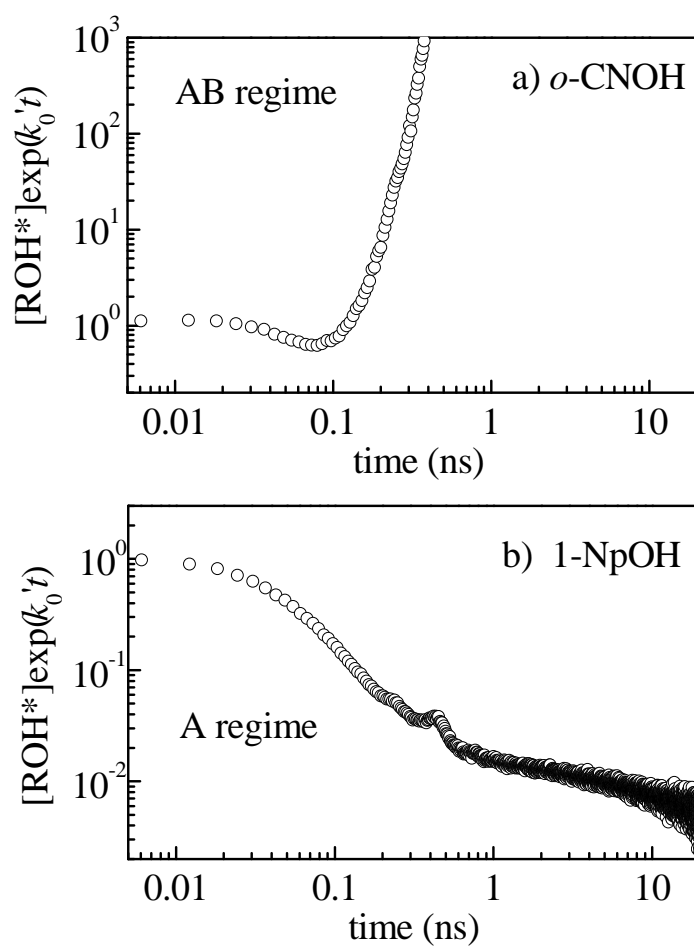
Figure IV-10. Log-log plot of corrected fluorescence decay curve, [ROH*]exp(k_0') of a) *o*-CNOH in H_2O (pH 2.9) and b) 1-NpOH in H_2O (pH 6.0) at 293K.

References

[1] (a) Förster, T. *Naturwiss.* **1949**, *36*, 186. (b) Förster, T. *Z. Elektrochem.* **1950**, *54*, 42, 531.

[2] (a) Weller, A. *Z. Elektrochem.* **1952**, *56*, 662. (b) Weller, A. *Z. Elektrochem.* **1954**, *58*, 849.

[3] Martynov, I. Y.; Demyashkevich, A. B.; Uzhinov, B. M.; Kuz'min, M. G. *Russ. Chem. Rev.* (*Usp. Khim.*) **1977**, *46*, 3.

[4] Shizuka, H. *Acc. Chem. Res.* **1985**, *18*, 141.

[5] Kosower, E. M.; Huppert, D. *Ann. Rev. Phys. Chem.* **1986**, *37*, 127.

[6] Alnaut, L. G.; Formosinho, S. J. *J. Photochem. Photobiol. A: Chem.* **1993**, *75*, 1.

[7] Mishra, A. K. Fluorescence of Excited Singlet State Acids in Certain Organized Media: *Applications as Molecular Probes, Eds. V. Ramamurthy and K. S. Schanze, in Understanding and Manipulating Excited State Processes, Molecular and Supramolecular Photochemistry Series*, Marcel Dekker, Inc., New York, 2001, Vol. 8, Chap. 10.

[8] Caldin, E. F. in The Mechanisms of Fast Reactions in Solution, IOS Press, Amsterdam, 2001, Chap.8.

[9] Tolbert, L. M.; Solntsev, K. M. *Acc. Chem Res.* **2002**, *35*, 19.

[10] Agmon, N. *J. Phys. Chem. A* **2005**, *109*, 13.

[11] Shizuka, H.; Tobita, S. Proton Transfer Reactions in the Excited States, In *Organic Photochemistry and Photophysics, Molecular and Supramolecular Photochemistry Series Vol. 14*, Ramamurthy, V., Schanze, K. S. Eds.; CRC Press: Boca Raton, 2006; Chapter 2.

[12] Lee, J.; Robinson, G. W.; Webb, S. P.; Philips, L. A.; Clark, J. H. *J. Am. Chem. Soc.* **1986**, *108*, 6538.

[13] Webb, S. P.; Philips, L. A.; Yeh, S. W.; Tolbert, L. M.; Clark, J. H. *J. Phys. Chem.* **1986**, *90*, 5154.

[14] (a) Robinson, G. W.; Thistlethwaite, P. J.; Lee, J. *J. Phys. Chem.* **1986**, *90*, 4224. (b) Robinson, G. W. *J. Phys. Chem.* **1991**, *95*, 10386.

[15] Poles, W.; Cohen, B.; Huppert, D.; *Isr. J. Chem.* **1999**, *39*, 347.

[16] Solntsev, K. M.; Huppert, D.; Agmon, N.; Tolbert, L. M. *J. Phys. Chem. A* **2000**, *104*, 4658.

[17] Clower, C.; Solntsev, K. M.; Kowalik, J.; Tolbert, L. M.; Huppert, D. *J. Phys. Chem. A* **2002**, *106*, 3114.

[18] Genosar, L.; Leiderman, P.; Koifman, N,; Huppert, D. *J. Phys. Chem. A* **2004**, *108*, 1779.

[19] Wehry, E. L.; Rogers, L. B. *J. Am. Chem. Soc.* **1965**, *87*, 4234

[20] Schulman, S. G.; Vincent, W. R.; Underberg, W. J. M. *J. Phys. Chem.* **1981**, *85*, 4068.

[21] Chalfie, M; Kain, S. *Green Fluorescent Protein: Properties, Applications, and Protocols*; Wiley-Liss: New York, 1998.

[22] Tsien, R. Y. *Annu. Rev. Biochem.* **1998**, *67*, 509.

[23] Chattoraj, M.; King, B. A.; Bublitz, G. U.; Boxer, S. G. Proc. *Natl. Acad. Sci. U.S.A.* **1996**, *93*, 8362.

[24] Stoner-Ma, D.; Jaye, A. A.; Ronayne, K. L.; Nappa, J.; Meech, S. R.; Tonge, P. J. *J. Am. Chem. Soc.* **2008**, *130*, 1227.

[25] Leiderman, P.; Gepshtein, R.; Tsimberov, I.; Huppert, D. *J. Phys. Chem. B* **2008**, *112*, 1232.

[26] Gepshtein, R.; Leiderman, P.; Huppert, D. *J. Phys. Chem. B* **2008**, *112*, 7203.

[27] Eaton, D. F.; *Pure Appl. Chem.* **1988**, *60*, 1107.

[28] Perichet, R. G.; Chaperon, R.; Pouyet, B. *J. Photochem.* **1980**, *13*, 67.

[29] Oshima, J.; Shiobara, S.; Naoumi, H.; Kaneko, S.; Yoshihara, T.; Mishra. A. K.; Tobita, S. *J. Phys. Chem. A* **2006**, *110*, 4629.

[30] Tsutsumi, K.; Shizuka, H. *Z. Phys. Chem. Neue Folge*, **1980**, *122*, 129.

[31] Wang, H.; Wang, X.; Li, X.; Zhang, C. *J. Molec. Struct.* **2006**, *770*, 107.

[32] Grabner, G.; Köhler, G.; Zechner, J.; Getoff, N. *J. Phys. Chem.* **1980**, *84*, 3000.

[33] Pál, K.; Kállay, M.; Köhler, G.; Zhang, H.; Bitter, I.; Kubinyi, M.; Vidóczy, T.; Grabner, G. *ChemPhysChem.* **2007**, *8*, 2627.

[34] Shiobara, S.; Tajima, S. Tobita, S. *Chem. Phys. Lett.* **2003**, *380*, 673.

[35] (a) Agmon, N. *J. Chem. Phys.* **1988**, *89*, 1524. (b) Gopich, I. V.; Solntsev, K. M.; Agmon, N. *J. Chem. Phys.* **1999**, *110*, 2164. (c) Solntsev, K. M.; Huppert, D.; Agmon, N. *Phys. Rev. Lett.* **2001**, *86*, 3427.

[36] (a) Braslavsky, S. E.; Heibel, G. E. *Chem. Rev.* **1992**, *92*, 1381. (b) Churio, M. S.; Angermund, K. P.; Braslavsky, S. E. *J. Phys. Chem.* **1994**, *98*, 1776. (c) Gensch, T. ; Braslavsky, S. E. *J. Phys. Chem. B* **1997**, *101*, 101. (d) Small J. R. Libertini, L. J.; Small, E. W. *Biophys. Chem.* **1992**, *42*, 29. (e) Borsarelli, C. D.; Bertolotti, S. G.; Previtali, C. M *Photochem. Photobiol. Sci.* **2003**, *2*, 791.

[37] Losi, A.; Viappiani, C. *Chem. Phys. Lett.* **1998**, *289*, 500.

[38] Hamann, S. D.; Linton, M. *J. Chem. Soc. Faraday Trans. 1* **1974**, *70*, 2239.

[39] Hopkins Jr., H. P.; Duer, W. C.; Millero, F. J. *J. Solution Chem.* **1976**, *5*, 263.

[40] Rønne, C.; Thrane, L.; Åstrand, P.-O.; Wallqvist, A.; Mikkelsen, K. V.; Keiding, S. R. *J. Chem. Phys.* **1997**, *107*, 5319.

[41] Rønne, C.; Åstrand, P.-O.; Keiding, S. R. *Phys. Rev. Lett.* **1999**, *82*, 2888.

[42] Rønne, C.; Keiding, S. R. *J. Mol. Liquids* **2002**, *101*, 199.

[43] Cohen, B.; Leiderman, P.; Huppert, D. *J. Phys. Chem. A* **2002**, *106*, 11115.

[44] (a) Granucci, G.; Hynes, J. T.; Millie, P.; Tran-Thi, T. H. *J. Am. Chem. Soc.* **2000**, *122*, 12243. (b) Hynes, J. T.; Tran-Thi, T. H.; Granucci, G. *J. Photochem. Photobiol. A* **2002**, *154*, 3.

[45] Staib, A.; Borgis, D.; Hynes, J. T. *J. Chem. Phys.* **1995**, *102*, 2487.

[46] (a) Lewis, F. D.; Crompton, E. M. *J. Am. Chem. Soc.* **2003**, *125*, 4044. (b) Crompton, E. M.; Lewis, F. D. *Photochem. Photobiol. Sci.* **2004**, *3*, 660. (c) Lewis, F. D.; Sinks, L. E.; Weigel, W.; Sajimon, M. C.; Crompton, E. M. *J. Phys. Chem. A* **2005**, *109*, 2443.

[47] Pines, E.; Pines, D.; Barak, T.; Magnes, B. -Z. Tolbert, L. M. Haubrich, J. E. *Ber. Bunsenges. Phys. Chem.* **1998**, *102*, 511.

[48] Poizat, O.; Bardez, E.; Buntinx, G.; Alain, V. *J. Phys. Chem. A* **2004**, *108*, 1873.

[49] Mandal, D.; Tahara, T.; Meech, S. R. *J. Phys. Chem. B* **2004**, *108*, 1102.

[50] Gepshtein, R.; Huppert, D.; Agmon, N. *J. Phys. Chem. B* **2006**, *110*, 4434.

[51] Tran-Thi, T. H.; Prayer, C.; Millie, P.; Uznanski, P.; Hynes, J. T. *J. Phys. Chem. A* **2002**, *106*, 2244.

[52] Tran-Thi, T. H.; Gustavsson, T.; Prayer, C.; Pommeret, S.; Uznanski, P.; Hynes, J. T. *Chem. Phys. Lett.* **2000**, *229*, 421.

[53] Timoneda, J. J.; Hynes, J. T. *J. Phys. Chem.* **1991**, *95*, 10431.

[54] Pines, E.; Huppert, D. *Chem. Phys. Lett.* **1986**, *126*, 88.

[55] Pines, E.; Huppert, D. *J. Chem. Phys.* **1986**, *84*, 3576.

[56] Agmon, N.; Pines, E.; Huppert, D. *J. Chem. Phys.* **1988**, *88*, 5631.

[57] Pines, E.; Huppert, D.; Agmon, N. *J. Chem. Phys.* **1988**, *88*, 5620.

[58] Cohen, B.; Huppert, D. *J. Phys. Chem. A* **2002**, *106*, 1946.

[59] Agmon, N.; Goldberg, S. Y.; Huppert, D. *J. Mol. Liquids* **1995**, *64*, 161.

Chapter V

Summary

In this thesis, the excited-state proton dissociation reactions of phenol and its derivatives (*o*-, *m*-, and *p*-trifluoromethylphenols and *o*-, *m*-, and *p*-cyanophenols) in water were investigated by means of steady-state and time-resolved fluorescence spectroscopy and time-resolved photoacoustic technique.

In Chapter Ⅲ, the proton transfer reactions to solvent from electronically excited *o*-, *m*-, and *p*-trifluoromethylphenols (TFOHs) in water were investigated by picosecond time-resolved fluorescence measurements. The introduction of a moderately electron-withdrawing CF_3 group into the aromatic ring of phenol enhanced the fluorescence quantum yield of the deprotonated anion and the dual fluorescence was observed in TFOHs. The rate constants for the proton dissociation of *o*-, *m*-, and *p*-TFOH were obtained to be 2.2 x 10^9, 8.6 x 10^8, and 2.5 x 10^8 s^{-1}, respectively. The activation energy and the deuterium isotope effect ($k_{dis}^H/k_{dis}^D = 3.0$–$6.0$) were ascribed to the proton motion along the proton-transfer coordinate. The isotope effect on the k_{dis} value in *p*-TFOH depended on temperature more strongly than those in *o*-TFOH and *m*-TFOH.

In Chapter IV, the excited-state proton transfer (ESPT) to solvent from phenol (PhOH) and cyanophenols (CNOHs) in water was studied by time-resolved fluorescence and photoacoustic mesurements. A characteristic property of PhOH and CNOHs was that the fluorescence quantum yields of the deprotonated forms are remarkably small ($\leq 10^{-3}$), and the lifetimes are extremely short (≤ 30ps). Time-resolved fluorescence measurements for PhOH, CNOHs and their methoxy analogues at 298K indicated that *o*- and *m*-cyanophenols (*o*- and *m*-CNOH) undergo rapid ESPT to solvent water with rate constants of 6.6 x 10^{10} and 2.6 x 10^{10} s^{-1}, respectively, while the fluorescence properties of PhOH and *p*-CNOH does not exhibit clear evidence of the ESPT reaction. Photoacoustic measurements showed that photoexcitation of *o*- and

m-CNOH in water results in negative volume changes, supporting the occurrence of ESPT to produce a geminate ion pair. In contrast, the volume contractions for the PhOH and *p*-CNOH solutions were negligibly small, which also indicated that in these compounds the ESPT does not occur. The volume change per absorbed Einstein (ΔV_r) for *o*-CNOH was obtained to be -5.0 mL Einstein^{-1}, which was much smaller than the estimated volume contraction per photoconverted mole (ΔV_R). This suggested that the geminate recombination between the ejected proton and the cyanophenolate anion occurs after rapid deactivation of the excited ion pair. In the temperature range between 275 and 323K, the proton dissociation rates of *o*- and *m*-CNOH in H_2O and D_2O were slower than the solvent relaxation rates evaluated from the Debye dielectric relaxation time, indicating that the overall rate constant is determined mainly by the proton motion along the reaction coordinate.

Acknowledgments